Numerical analysis of superconducting phases in the extended Hubbard model with non-local pairing

University of Pisa, a.y. 2025-2026

Alessandro Gori*

Thesis for the Master's degree in Physics

Abstract

[To be continued...]

Contents

Draft: August 24, 2025

*a.gori23@studenti.unipi.it / nepero27178@github.com

List of symbols and abbreviations

AF	Anti-Ferromagnetic
BCS	Bardeen-Cooper-Schrieffer (theory)
DoF	Degree of Freedom
HF	Hartree-Fock
MFT	Mean-Field Theory
SC	Superconductor
T_c	Critical temperature

Introduction

This thesis project is about my favorite ice cream flavor. [To be continued...]

Chapter 1

Theoretical introduction

[To be continued...]

1.1 Antiferromagnetic ordering in the Hubbard model

Consider the ordinary Hubbard model:

$$\hat{H} = -t \sum_{\langle ij \rangle} \sum_{\sigma} \hat{c}^{\dagger}_{i\sigma} \hat{c}_{j\sigma} + U \sum_{i} \hat{n}_{i\uparrow} \hat{n}_{i\downarrow} \qquad t, U > 0 \tag{1.1}$$

The two competing mechanisms are site-hopping of amplitude t and local repulsion of amplitude U. For this model defined **on a bipartite lattice at half filling** and fixed electron number, it is well known [6] that, below a certain critical temperature T_c and above some (small) critical repulsion U_c/t, the ground-state acquires antiferromagnetic (AF) long-range ordering. schematically depicted in Fig. 1.1a. The mechanism for the formation of the AF phase takes advantage of virtual hopping, as described in App. A; the Mean-Field Theory (MFT) treatment of ferromagnetic-antiferromagnetic orderings in 2D Hubbard lattices is discussed in App. B.

In this chapter the discussion is limited to the two-dimensional square lattice Hubbard model. The lattice considered has L_ℓ sites on side $\ell = x, y$, thus a total of $L_x L_y$ sites. The total number of single electron states is given by $D = 2L_x L_y$. All theoretical discussion neglects border effects, thus considering $D \to +\infty$.

1.2 The Extended Fermi-Hubbard model

The Extended Fermi-Hubbard model is defined by:

$$\hat{H} = -t \sum_{\langle ij \rangle} \sum_{\sigma} \hat{c}^{\dagger}_{i\sigma} \hat{c}_{j\sigma} + U \sum_{i} \hat{n}_{i\uparrow} \hat{n}_{i\downarrow} - V \sum_{\langle ij \rangle} \sum_{\sigma\sigma'} \hat{n}_{i\sigma} \hat{n}_{j\sigma'} \tag{1.2}$$

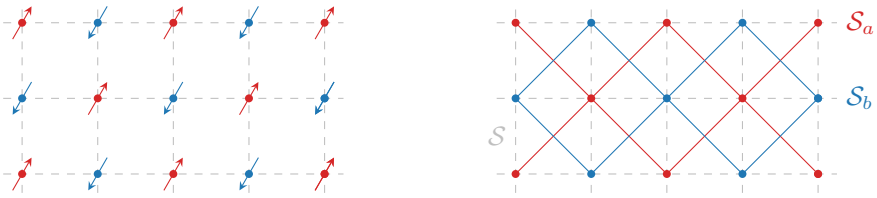

a | Antiferromagnetic phase. b | Polarized sublattices.

Figure 1.1 | Schematic representation of the AF phase. Fig. 1.1a shows a portion of the square lattice with explicit representation of the spin for each site. Fig. 1.1b divides the square lattice $\mathcal{S}$ in two polarized sublattices $\mathcal{S}_a$, $\mathcal{S}_b$. The AF phase results from the interaction of two inversely polarized "ferromagnetic" square lattices.

Note that, on a square lattice, we can perform the summation over NN just as

$$\sum_{\langle ij \rangle} \equiv \sum_{i \in \mathcal{S}_a} \left[\delta_{j=i+\delta_x} + \delta_{j=i-\delta_x} + \delta_{j=i+\delta_y} + \delta_{j=i-\delta_y} \right]$$

where notation of Fig. 1.1b has been used. The last term represents an effective attraction between neighboring electrons, of amplitude V. Such an interaction is believed [1] necessary to describe the insurgence of high-T_c superconductivity in cuprate SCs. [To be continued...]

1.2.1 Experimental insight on NN attraction

Todo:

- High T_c SC in cuprates;
- Experimental evidence of topological SC;
- Insertion of the non-local attraction;

Chapter 2

Mean-field theory solution

This chapter is devoted to develop a rough mean field approximation of the Extended Hubbard model of Eq. (1.2),

$$\hat{H} = \underbrace{-t \sum_{\langle ij \rangle} \sum_{\sigma} \hat{c}^{\dagger}_{i\sigma} \hat{c}_{j\sigma}}_{\hat{H}_t} + \underbrace{U \sum_{i} \hat{n}_{i\uparrow} \hat{n}_{i\downarrow}}_{\hat{H}_U} \underbrace{- V \sum_{\langle ij \rangle} \sum_{\sigma\sigma'} \hat{n}_{i\sigma} \hat{n}_{j\sigma'}}_{-\hat{H}_V}$$

Mean Field Theory (MFT) is a widely used and simple theoretical tool, often sufficient to describe the leading orders in phase transition phenomena of Many-Body Physics. Here MFT is employed following the path of Bardeen-Cooper-Schrieffer (BCS) theory in describing conventional s-wave superconductivity. As will be thoroughly described, the lattice spatial structure directly influences the topology of the gap function, giving rise to anisotropic pairing. Sec. 2.1 studies the non-local attraction in real-space, while Sec. 2.2 moves to reciprocal space and gives a self-consistent MFT solution. Finally, numerical results are exposed in Sec. 2.3.

2.1 Mean-Field theory real space description

In this section, an analytic discussion of the real-space hamiltonian of Eq. (1.2) is given. The first part focuses on the non-local interaction V, expected to be source of superconductivity; the second part on the local interaction U, known to be source of Slater-like anti-ferromagnetism, as described in App. B.

2.1.1 Mean-field treatment of the non-local term

Consider the non-local term,

$$\hat{H}_V \equiv -V \sum_{\langle ij \rangle} \sum_{\sigma\sigma'} \hat{n}_{i\sigma} \hat{n}_{j\sigma'} \tag{2.1}$$

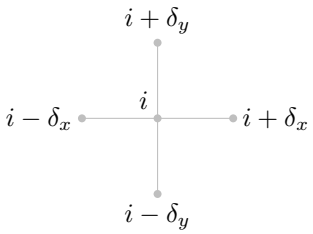

Figure 2.1 | Schematic representation of the four NNs of a given site i for a planar square lattice.

Evidently the hamiltonian can be decomposed in various spin terms,

$$\begin{aligned}\hat{H}_V &= \sum_{\sigma\sigma'} \hat{H}_V^{\sigma\sigma'} \\ &= \underbrace{\hat{H}_V^{\uparrow\uparrow} + \hat{H}_V^{\downarrow\downarrow}}_{\text{Ferromagnetic}} + \underbrace{\hat{H}_V^{\uparrow\downarrow} + \hat{H}_V^{\downarrow\uparrow}}_{\text{Anti-ferromagnetic}}\end{aligned}$$

Evidently, to carry out a summation over nearest neighbors $\langle ij \rangle$ of a square lattice means precisely to sum over all links of the lattice. Then we can identify the generic AF term $\hat{H}_V^{\sigma\overline{\sigma}}$ as the one collecting the σ operators of sublattice $\mathcal{S}_a$ and $\overline{\sigma}$ operators of sublattice $\mathcal{S}_b$. At half-filling, as described in Sec. 1.1, the ground-state leading contribution will be the antiferromagnetic state, with the square lattice decomposed in two oppositely polarized square lattices with spacing increased by a factor $\sqrt{2}$. Then, it is to be expected that on this configuration the ferromagnetic contributions are suppressed[1]. Anyways, the calculation will be carried out considering both terms. The AF non-local interactions can be written as a sum of terms over just one of the two sublattices $\mathcal{S}_a$ and $\mathcal{S}_b$, oppositely polarized in the AF configuration (see Fig. 1.1b)

$$\begin{aligned}\hat{H}_V^{(\mathrm{AF})} &= \overbrace{\sum_{i\in\mathcal{S}_a} \hat{h}_V^{(i)}}^{\hat{H}_V^{\uparrow\downarrow}} + \overbrace{\sum_{i\in\mathcal{S}_b} \hat{h}_V^{(i)}}^{\hat{H}_V^{\downarrow\uparrow}} \\ &= \sum_{i\in\mathcal{S}} \hat{h}_V^{(i)}\end{aligned} \qquad \hat{h}_V^{(i)} = -V \sum_{\ell=x,y} (\hat{n}_{i\uparrow}\hat{n}_{i+\delta_\ell\downarrow} + \hat{n}_{i\uparrow}\hat{n}_{i-\delta_\ell\downarrow})$$

Here the notation of Fig. 1.1b is used. The two-dimensional lattice is regular-square. For each site i in a given sublattice, the nearest neighbors sites are four – all in the other sublattice. The notation used is $i \pm \delta_x$, $i \pm \delta_y$ as in Fig. 2.1. Similarly, the Ferromagnetic hamiltonian decomposes as

$$\hat{H}_V^{(\mathrm{F})} = -V \sum_{i\in\mathcal{S}_a} \sum_{\ell=x,y} \sum_{\sigma} (\hat{n}_{i\sigma}\hat{n}_{i+\delta_\ell\sigma} + \hat{n}_{i\sigma}\hat{n}_{i-\delta_\ell\sigma})$$

Note here the summation only on one sublattice. As will be shown in Sec. 2.2.5, under MFT it makes sense to approximate

$$\hat{H}_V \simeq \hat{H}_V^{(\mathrm{AF})}$$

thus neglecting ferromagnetic contribution to Cooper instability. The non-local interaction contribution to energy, as a function of the $T = 0$ full hamiltonian ground-state[2] $|\Psi\rangle$, is given by

$$\begin{aligned}E_V[\Psi] &= \langle\Psi|\hat{H}_V|\Psi\rangle \\ &= -V \sum_{i\in\mathcal{S}} \sum_{\ell=x,y} \langle \hat{n}_{i\uparrow}\hat{n}_{i+\delta_\ell\downarrow} + \hat{n}_{i\uparrow}\hat{n}_{i-\delta_\ell\downarrow}\rangle\end{aligned}$$

Shorthand notation has been used: $\langle\Psi|\cdot|\Psi\rangle = \langle\cdot\rangle$. Consider one specific term, say, $\hat{n}_{i\uparrow}\hat{n}_{i+\delta_x\downarrow}$. Wick's Theorem states that, if the expectation value is performed onto a coherent state,

$$\begin{aligned}\langle \hat{n}_{i\uparrow}\hat{n}_{i+\delta_x\downarrow}\rangle &= \langle \hat{c}_{i\uparrow}^\dagger \hat{c}_{i+\delta_x\downarrow}^\dagger \hat{c}_{i+\delta_x\downarrow}\hat{c}_{i\uparrow}\rangle \\ &= \underbrace{\langle \hat{c}_{i\uparrow}^\dagger \hat{c}_{i+\delta_x\downarrow}^\dagger\rangle\langle \hat{c}_{i+\delta_x\downarrow}\hat{c}_{i\uparrow}\rangle}_{\text{Cooper}} - \underbrace{\langle \hat{c}_{i\uparrow}^\dagger \hat{c}_{i+\delta_x\downarrow}\rangle\langle \hat{c}_{i+\delta_x\downarrow}^\dagger \hat{c}_{i\uparrow}\rangle}_{\text{Fock}} + \underbrace{\langle \hat{c}_{i\uparrow}^\dagger \hat{c}_{i\uparrow}\rangle\langle \hat{c}_{i+\delta_x\downarrow}^\dagger \hat{c}_{i+\delta_x\downarrow}\rangle}_{\text{Hartree}}\end{aligned}$$

As a first approximation, the theorem is assumed to hold (which, in a BCS-like fashion, is equivalent to assuming for the ground-state to be a coherent state). The last two terms account for single-particle interactions with a background field; they are relevant in the Hartree-Fock scheme, being

[1] This is also due to superexchange stabilization: the triplet contribution to hamiltonian is suppressed, and this cancels out the ferromagnetic terms $\hat{H}_V^{\sigma\sigma}$ while privileging the singlet configuration of the anti-ferromagnetic terms $\hat{H}_V^{\sigma\overline{\sigma}}$.

[2] Extensions to finite temperatures is simple: minimization must be carried out on free energy, while expectation values must be taken in a thermodynamic fashion.

direct-exchange contributions to single particle energies. The first term accounts for non-local electrons pairing, mimicking the Cooper term of BCS theory. The core assumption, here, is that only one of the HF and Bogoliubov pairings survive. Appendix B shows a situation dominated by HF terms. Here, I assume the symmetry to be broken by a Cooper term. Energy then is cast to the form

$$E_V[\Psi] = -V \sum_{i\in\mathcal{S}} \sum_{\ell=x,y} \left[\langle \hat{c}^\dagger_{i\uparrow} \hat{c}^\dagger_{i+\delta_\ell\downarrow} \rangle \langle \hat{c}_{i+\delta_\ell\downarrow} \hat{c}_{i\uparrow} \rangle + \langle \hat{c}^\dagger_{i\uparrow} \hat{c}^\dagger_{i-\delta_\ell\downarrow} \rangle \langle \hat{c}_{i-\delta_\ell\downarrow} \hat{c}_{i\uparrow} \rangle \right]$$

The ground-state must realize the condition

$$\frac{\delta}{\delta \langle \Psi |} E[\Psi] = 0$$

being $E[\Psi]$ the total energy (made up of the three terms of couplings t, U and V). [Expand derivation?] The functional derivative must be carried out in a variational fashion including a Lagrange multiplier, the latter accounting for state-norm conservation, as is done normally in deriving the Hartree-Fock approximation for the eigenenergies of the electron liquid [4, 5]. This approach leads to the conclusion that the (coherent) ground-state of the system must be an eigenstate of the mean-field effective hamiltonian:

$$\begin{aligned} \hat{H}^{(\mathrm{e})} = & -t \sum_{\langle ij \rangle} \sum_{\sigma} \hat{c}^\dagger_{i\sigma} \hat{c}_{j\sigma} + U \sum_{i\in\mathcal{S}} \hat{n}_{i\uparrow} \hat{n}_{i\downarrow} \\ & - V \sum_{i\in\mathcal{S}} \sum_{\ell=x,y} \sum_{\delta=\pm\delta_\ell} \left[\langle \hat{c}^\dagger_{i\uparrow} \hat{c}^\dagger_{i+\delta\downarrow} \rangle \hat{c}_{i+\delta\downarrow} \hat{c}_{i\uparrow} + \mathrm{h.c.} \right] \end{aligned} \tag{2.2}$$

The pairing correlation function is defined across each bond as the pairing expectation

$$g_{ij} \equiv \langle \hat{c}^\dagger_{i\uparrow} \hat{c}^\dagger_{j\downarrow} \rangle$$

The effective hamiltonian reads:

$$\hat{H}^{(\mathrm{e})} = -t \sum_{\langle ij \rangle} \sum_{\sigma} \hat{c}^\dagger_{i\sigma} \hat{c}_{j\sigma} + U \sum_{i\in\mathcal{S}} \hat{n}_{i\uparrow} \hat{n}_{i\downarrow} - V \sum_{\langle ij \rangle} \left[g_{ij} \hat{c}_{j\downarrow} \hat{c}_{i\uparrow} + g^*_{ij} \hat{c}^\dagger_{i\uparrow} \hat{c}^\dagger_{j\downarrow} \right] \tag{2.3}$$

As in standard BCS theory, this hamiltonian – being quadratic in the electronic operators – can be diagonalized via a Bogoliubov rotation. Superconducting pairing can arise both from the local U term and from the non-local V term. In next sections it is assumed the V term generates dominant superconductivity via its weak non-local pairing.

2.1.2 Mean-field treatment of the local term

The mean-field description of the local (on-site) U interaction is given in detail in App. B, along with a simple numerical analysis of the insurgence of antiferromagnetic ordering in a Hartree-Fock approximation scheme. Here the Cooper pairing is likewise assumed to dominate. Performing an analysis analogous to the one carried out in last section, we get the decoupling

$$U \sum_{i\in\mathcal{S}} \hat{n}_{i\uparrow} \hat{n}_{i\downarrow} \simeq U \sum_{i\sigma} \left[f_i \hat{c}_{i\downarrow} \hat{c}_{i\uparrow} + f^*_i \hat{c}^\dagger_{i\uparrow} \hat{c}^\dagger_{i\downarrow} \right]$$

being

$$f_i \equiv \langle \hat{c}^\dagger_{i\uparrow} \hat{c}^\dagger_{i\downarrow} \rangle$$

Collect f and g in the unique function of two variables:

$$C(i,j) = \begin{cases} f_i & \text{if} \quad i = j \\ g_{ij} & \text{if} \quad |i-j| = 1 \\ (\cdots) & \text{otherwise} \end{cases}$$

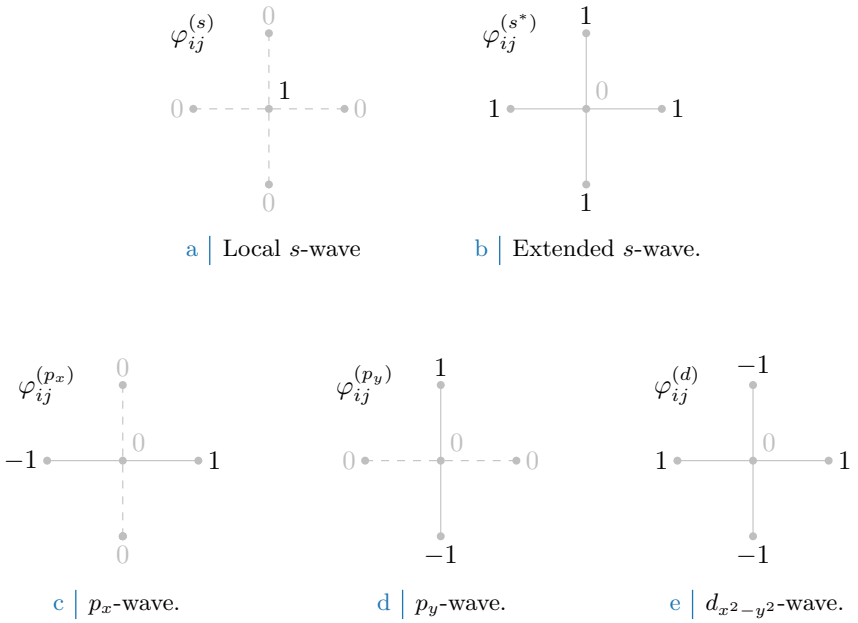

a | Local s-wave b | Extended s-wave.

c | p_x-wave. d | p_y-wave. e | $d_{x^2-y^2}$-wave.

Figure 2.2 | Form factors at different topologies, as listed in Tab. 2.1. In figures five sites are represented: the hub site i and its four NN. Solid lines represent non-zero values for $\varphi_{\boldsymbol{\delta}}$, while dashed lines represent vanishing factors.

which expresses the generic correlator $\langle \hat{c}_{i\uparrow}^\dagger \hat{c}_{j\downarrow}^\dagger \rangle$. The correlator for $|i-j|>1$ is left unexpressed, and supposed to be subdominant. The decoupled hamiltonian, apart from pure energy shifts and suppressed terms, is given by

$$\hat{H}^{(\mathrm{e})} = -t \sum_{\langle ij \rangle} \sum_{\sigma} \hat{c}_{i\sigma}^\dagger \hat{c}_{j\sigma} + U \sum_i \left[f_i \hat{c}_{i\downarrow} \hat{c}_{i\uparrow} + f_i^* \hat{c}_{i\uparrow}^\dagger \hat{c}_{i\downarrow}^\dagger \right] - V \sum_{\langle ij \rangle} \left[g_{ij} \hat{c}_{j\downarrow} \hat{c}_{i\uparrow} + g_{ij}^* \hat{c}_{i\uparrow}^\dagger \hat{c}_{j\downarrow}^\dagger \right] \tag{2.4}$$

[To be continued...]

2.1.3 Topological correlations

Topology plays an important role in establishing SC, giving rise to anisotropic pairing as well as real space structures for the Cooper pairs. The correlator g_{ij} is a function of position, specifically of its variables difference $\boldsymbol{\delta} \equiv \mathbf{x}_j - \mathbf{x}_i$. Over the square lattice with NN interaction, the latter can assume four values: $\boldsymbol{\delta} = \pm\boldsymbol{\delta}_x, \pm\boldsymbol{\delta}_y$. For a function of space defined over the four rim sites $\mathbf{x}_i \pm \boldsymbol{\delta}_\ell$ of Fig. 2.1, various symmetry structures can be defined under the planar rotations group SO(2). In other words, the function $g_{\boldsymbol{\delta}}$ can be decomposed in planar harmonics (which are simply the sine-cosine basis). Equivalently, given two NN sites i, j

$$g_{ij} = \sum_\gamma g^{(\gamma)} \varphi_{ij}^{(\gamma)}$$

where $g^{(\gamma)}$ are the g_{ij} symmetries-decomposition coefficients while $\varphi_{ij}^{(\gamma)}$ are the form factors listed in Tab. 2.1, a simple orthonormal rearrangement of the harmonics basis.

SC is established with a given symmetry – which means, symmetry breaking in the phase transition proceeds in a specific channel. Conventional BCS superconductivity arises from the only possible spatial structure of the local pairing, s-wave – here appearing as a local term (Fig. 2.2a) and extended on a non-local term (Fig. 2.2b). Cuprates exhibit a tendency towards $d_{x^2-y^2}$ SC, while other materials towards p-wave types – eventually with some chirality, as is the case for $p_x \pm ip_y$ SCs. To establish SC under a certain symmetry γ means that Cooper pairs acquire said symmetry – which implies, for correlations, $g^{(\gamma')} = g^{(\gamma)} \delta_{\gamma\gamma'}$. and $g_{ij} \propto \varphi_{ij}^{(\gamma)}$.

Structure	Form factor	Graph
s-wave	$\varphi_{ij}^{(s)} = \delta_{ij}$	Fig. 2.2a
Extended s-wave	$\varphi_{ij}^{(s^*)} = \delta_{j=i+\delta_x} + \delta_{j=i-\delta_x} + \delta_{j=i+\delta_y} + \delta_{j=i-\delta_y}$	Fig. 2.2b
p_x-wave	$\varphi_{ij}^{(p_x)} = \delta_{j=i+\delta_x} - \delta_{j=i-\delta_x}$	Fig. 2.2c
p_y-wave	$\varphi_{ij}^{(p_y)} = \delta_{j=i+\delta_y} - \delta_{j=i-\delta_y}$	Fig. 2.2d
$d_{x^2-y^2}$-wave	$\varphi_{ij}^{(d)} = \delta_{j=i+\delta_x} + \delta_{j=i-\delta_x} - \delta_{j=i+\delta_y} - \delta_{j=i-\delta_y}$	Fig. 2.2e

Table 2.1 First four spatial structures for the correlation function $C(i,j)$. In the middle column, all spatial dependence is included in the δs, while $f^s, g^{(\gamma)} \in \mathbb{C}$. The last column indicates the graph representation of each contribution given in Fig. **??**. Subscript x^2-y^2 is omitted for notational clarity.

2.2 Mean-Field theory reciprocal space description

In this BCS-like approach, a self-consistent equation for the gap function must be retrieved in order to further investigate the model and extract the conditions for the formation of a superconducting phase with a given pairing topology. In order to do so, let me take a step back and perform explicitly the Fourier-transform of the various terms of Eq. 1.2.

2.2.1 Kinetic term

The kinetic part is trivial to transform. The followed convention is

$$\hat{c}_{j\sigma} = \frac{1}{\sqrt{L_x L_y}} \sum_{\mathbf{k}\in \mathrm{BZ}} e^{-i\mathbf{k}\cdot\mathbf{x}_j} \hat{c}_{\mathbf{k}\sigma}$$

Calculation is carried out in App. **??**. Let

$$\epsilon_{\mathbf{k}} \equiv -2t\left[\cos(k_x\delta_x) + \cos(k_y\delta_y)\right]$$

then we have

$$\begin{aligned} -t\sum_{\langle ij\rangle}\sum_{\sigma} \hat{c}_{i\sigma}^\dagger \hat{c}_{j\sigma} &= \sum_{\mathbf{k}\sigma} \epsilon_{\mathbf{k}} \hat{c}_{\mathbf{k}\sigma}^\dagger \hat{c}_{\mathbf{k}\sigma} \\ &= \sum_{\mathbf{k}} \epsilon_{\mathbf{k}} \left[\hat{c}_{\mathbf{k}\uparrow}^\dagger \hat{c}_{\mathbf{k}\uparrow} + \hat{c}_{\mathbf{k}\downarrow}^\dagger \hat{c}_{\mathbf{k}\downarrow}\right] \\ &= \sum_{\mathbf{k}} \epsilon_{\mathbf{k}} \left[\hat{c}_{\mathbf{k}\uparrow}^\dagger \hat{c}_{\mathbf{k}\uparrow} - \hat{c}_{-\mathbf{k}\downarrow} \hat{c}_{-\mathbf{k}\downarrow}^\dagger\right] \end{aligned}$$

In last passage I used fermionic anti-commutation rules and reversed the sign of the mute variable. This will become useful later.

2.2.2 Non-local attraction

Consider a generic bond, say, the one connecting sites j and $j \pm \delta_\ell$ (variable i is here referred to as the imaginary unit to avoid confusion). $\mathbf{x}_j$ is the 2D notation for the position of site j, while $\boldsymbol{\delta}_\ell$ is the 2D notation for the lattice spacing previously indicated as δ_ℓ. Fourier transform it according to the convention

$$\hat{c}_{j\sigma} = \frac{1}{\sqrt{L_x L_y}} \sum_{\mathbf{k}\in \mathrm{BZ}} e^{-i\mathbf{k}\cdot\mathbf{x}_j} \hat{c}_{\mathbf{k}\sigma}$$

Then:

$$\begin{aligned} \hat{n}_{j\uparrow}\hat{n}_{j\pm\delta_\ell\downarrow} &= \hat{c}_{j\uparrow}^\dagger \hat{c}_{j\pm\delta_\ell\downarrow}^\dagger \hat{c}_{j\pm\delta_\ell\downarrow} \hat{c}_{j\uparrow} \\ &= \frac{1}{(L_x L_y)^2} \sum_{\nu=1}^{4} \sum_{\mathbf{k}_\nu\in \mathrm{BZ}} e^{i[(\mathbf{k}_1+\mathbf{k}_2)-(\mathbf{k}_3+\mathbf{k}_4)]\cdot\mathbf{x}_j} e^{\pm i(\mathbf{k}_2-\mathbf{k}_3)\cdot\boldsymbol{\delta}_\ell} \hat{c}_{\mathbf{k}_1\uparrow}^\dagger \hat{c}_{\mathbf{k}_2\downarrow}^\dagger \hat{c}_{\mathbf{k}_3\downarrow} \hat{c}_{\mathbf{k}_4\uparrow} \end{aligned}$$

It follows,

$$\begin{aligned}\hat{h}_V^{(j)} &= -\frac{V}{(L_xL_y)^2}\sum_{\ell=x,y}\sum_{\nu=1}^{4}\sum_{\mathbf{k}_\nu\in\mathrm{BZ}} e^{i[(\mathbf{k}_1+\mathbf{k}_2)-(\mathbf{k}_3+\mathbf{k}_4)]\cdot\mathbf{x}_j} \\ &\qquad\qquad \times\left(e^{i(\mathbf{k}_2-\mathbf{k}_3)\cdot\boldsymbol{\delta}_\ell}+e^{-i(\mathbf{k}_2-\mathbf{k}_3)\cdot\boldsymbol{\delta}_\ell}\right)\hat{c}^\dagger_{\mathbf{k}_1\uparrow}\hat{c}^\dagger_{\mathbf{k}_2\downarrow}\hat{c}_{\mathbf{k}_3\downarrow}\hat{c}_{\mathbf{k}_4\uparrow} \\ &= -\frac{2V}{(L_xL_y)^2}\sum_{\ell=x,y}\sum_{\nu=1}^{4}\sum_{\mathbf{k}_\nu\in\mathrm{BZ}} e^{i[(\mathbf{k}_1+\mathbf{k}_2)-(\mathbf{k}_3+\mathbf{k}_4)]\cdot\mathbf{x}_j}\cos\left[(\mathbf{k}_2-\mathbf{k}_3)\cdot\boldsymbol{\delta}_\ell\right]\hat{c}^\dagger_{\mathbf{k}_1\uparrow}\hat{c}^\dagger_{\mathbf{k}_2\downarrow}\hat{c}_{\mathbf{k}_3\downarrow}\hat{c}_{\mathbf{k}_4\uparrow}\end{aligned}$$

The full non-local interaction is given by summing over all sites of $\mathcal{S}$. This gives back momentum conservation,

$$\frac{1}{L_xL_y}\sum_{j\in\mathcal{S}} e^{i[(\mathbf{k}_1+\mathbf{k}_2)-(\mathbf{k}_3+\mathbf{k}_4)]\cdot\mathbf{x}_j} = \delta_{\mathbf{k}_1+\mathbf{k}_2=\mathbf{k}_3+\mathbf{k}_4}$$

Let $\mathbf{k}_1+\mathbf{k}_2=\mathbf{k}_3+\mathbf{k}_4=\mathbf{K}$, and define $\mathbf{k}$, $\mathbf{k}'$ such that

$$\mathbf{k}_1\equiv\mathbf{K}+\mathbf{k}\qquad \mathbf{k}_2\equiv\mathbf{K}-\mathbf{k}\qquad \mathbf{k}_3\equiv\mathbf{K}-\mathbf{k}'\qquad \mathbf{k}_4\equiv\mathbf{K}+\mathbf{k}'\qquad \delta\mathbf{k}\equiv\mathbf{k}-\mathbf{k}'$$

Sums over these variables must be intended as over the Brillouin Zone (BZ). Then, finally

$$\begin{aligned}\hat{H}_V &\simeq \sum_{j\in\mathcal{S}}\hat{h}_V^{(j)} \\ &= -\frac{2V}{L_xL_y}\sum_{\ell=x,y}\sum_{\mathbf{K},\mathbf{k},\mathbf{k}'}\cos\left(\delta\mathbf{k}\cdot\boldsymbol{\delta}_\ell\right)\hat{c}^\dagger_{\mathbf{K}+\mathbf{k}\uparrow}\hat{c}^\dagger_{\mathbf{K}-\mathbf{k}\downarrow}\hat{c}_{\mathbf{K}-\mathbf{k}'\downarrow}\hat{c}_{\mathbf{K}+\mathbf{k}'\uparrow} \\ &= -\frac{2V}{L_xL_y}\sum_{\ell=x,y}\sum_{\mathbf{K},\mathbf{k},\mathbf{k}'}\left[\cos\left(\delta k_x\delta_x\right)+\cos\left(\delta k_y\delta_y\right)\right]\hat{c}^\dagger_{\mathbf{K}+\mathbf{k}\uparrow}\hat{c}^\dagger_{\mathbf{K}-\mathbf{k}\downarrow}\hat{c}_{\mathbf{K}-\mathbf{k}'\downarrow}\hat{c}_{\mathbf{K}+\mathbf{k}'\uparrow}\end{aligned}$$

Eventually, in the second passage the prefactor 2 can be absorbed by reintroducing the spin DoF[3]. Taking in the mean-field approximation (with Cooper pair symmetry breaking), we get

$$\hat{c}^\dagger_{\mathbf{K}+\mathbf{k}\uparrow}\hat{c}^\dagger_{\mathbf{K}-\mathbf{k}\downarrow}\hat{c}_{\mathbf{K}-\mathbf{k}'\downarrow}\hat{c}_{\mathbf{K}+\mathbf{k}'\uparrow} \simeq \langle\hat{c}^\dagger_{\mathbf{K}+\mathbf{k}\uparrow}\hat{c}^\dagger_{\mathbf{K}-\mathbf{k}\downarrow}\rangle\hat{c}_{\mathbf{K}-\mathbf{k}'\downarrow}\hat{c}_{\mathbf{K}+\mathbf{k}'\uparrow} + \hat{c}^\dagger_{\mathbf{K}+\mathbf{k}\uparrow}\hat{c}^\dagger_{\mathbf{K}-\mathbf{k}\downarrow}\langle\hat{c}_{\mathbf{K}-\mathbf{k}'\downarrow}\hat{c}_{\mathbf{K}+\mathbf{k}'\uparrow}\rangle + \cdots$$

Take e.g. $\langle\hat{c}^\dagger_{\mathbf{K}+\mathbf{k}\uparrow}\hat{c}^\dagger_{\mathbf{K}-\mathbf{k}\downarrow}\rangle$: the only non-zero contribution can come from the $\mathbf{K}=\mathbf{0}$ term, as will be discussed self-consistently in Sec. 2.2.5. Then finally:

$$\hat{H}_V \simeq \sum_{\mathbf{k},\mathbf{k}'} -V_{\mathbf{k}\mathbf{k}'}\left[\langle\hat{\phi}^\dagger_{\mathbf{k}}\rangle\hat{\phi}_{\mathbf{k}'}+\langle\hat{\phi}_{\mathbf{k}}\rangle\hat{\phi}^\dagger_{\mathbf{k}'}\right]$$

having I defined the pairing operator

$$\hat{\phi}_{\mathbf{k}}\equiv\hat{c}_{-\mathbf{k}\downarrow}\hat{c}_{\mathbf{k}\uparrow}\qquad \hat{\phi}^\dagger_{\mathbf{k}}\equiv\hat{c}^\dagger_{\mathbf{k}\uparrow}\hat{c}^\dagger_{-\mathbf{k}\downarrow}$$

and the two-body potential

$$V_{\mathbf{k}\mathbf{k}'} = \frac{2V}{L_xL_y}\left[\cos\left(\delta k_x\delta_x\right)+\cos\left(\delta k_y\delta_y\right)\right]$$

Now, consider the term

$$\begin{aligned}\cos\left(\delta k_x\delta_x\right)+\cos\left(\delta k_y\delta_y\right) &= \cos\left(k_x\delta_x\right)\cos\left(k'_x\delta_x\right)+\sin\left(k_x\delta_x\right)\sin\left(k'_x\delta_x\right) \\ &\quad +\cos\left(k_y\delta_y\right)\cos\left(k'_y\delta_y\right)+\sin\left(k_y\delta_y\right)\sin\left(k'_y\delta_y\right)\end{aligned}$$

For the sake of readability, the notations

$$c_\ell\equiv\cos\left(k_\ell\delta_\ell\right)\qquad s_\ell\equiv\sin\left(k_\ell\delta_\ell\right)\qquad c'_\ell\equiv\cos\left(k'_\ell\delta_\ell\right)\qquad s'_\ell\equiv\sin\left(k'_\ell\delta_\ell\right)$$

[3] Justification can be given in two ways: either commutating appropriately the $\hat{c}$ operators, or by carrying out the previous space sums independently over the two sublattices.

Structure	Structure factor	Graph
s-wave	$\varphi_{\mathbf{k}}^{(s)} = 1$	Fig. 2.2a
Extended s-wave	$\varphi_{\mathbf{k}}^{(s^*)} = \cos k_x + \cos k_y$	Fig. 2.2b
p_x-wave	$\varphi_{\mathbf{k}}^{(p_x)} = i \sin k_x$	Fig. 2.2c
p_y-wave	$\varphi_{\mathbf{k}}^{(p_y)} = i \sin k_y$	Fig. 2.2d
$d_{x^2-y^2}$-wave	$\varphi_{\mathbf{k}}^{(d)} = \cos k_x - \cos k_y$	Fig. 2.2e

Table 2.2 | Structure factors derived from the correlation structures of Tab. **??**. The functions hereby defined are orthogonal, and define the non-local topological effective potential as $V_{\mathbf{k}-\mathbf{k}'}^{(\gamma)} \equiv V \varphi_{\mathbf{k}-\mathbf{k}'}^{(\gamma)} / L_x L_y$.

are used. Group the four terms above,

$$\underbrace{\left(c_x c'_x + c_y c'_y\right)}_{\text{Symmetric}} + \underbrace{\left(s_x s'_x + s_y s'_y\right)}_{\text{Anti-symmetric}} \tag{2.5}$$

The first two exhibit inversion symmetry for both arguments $\mathbf{k}$, $\mathbf{k}'$; the second two exhibit anti-symmetry. Decoupling the symmetric part,

$$c_x c'_x + c_y c'_y = (c_x + c_y)(c'_x + c'_y) + (c_x - c_y)(c'_x - c'_y)$$

which finally gives:

$$\begin{aligned} \cos(\delta k_x \delta_x) + \cos(\delta k_y \delta_y) = {} & (c_x + c_y)(c'_x + c'_y) && (s^*\text{-wave}) \\ & + s_x s'_x && (p_x\text{-wave}) \\ & + s_y s'_y && (p_y\text{-wave}) \\ & + (c_x - c_y)(c'_x - c'_y) && (d_{x^2-y^2}\text{-wave}) \end{aligned}$$

In other words, the two-body potential decomposes as

$$\begin{aligned} V_{\mathbf{k}\mathbf{k}'} &= \sum_{\gamma} V^{(\gamma)} \varphi_{\mathbf{k}}^{(\gamma)} \varphi_{\mathbf{k}'}^{(\gamma)*} \qquad \text{where} \quad \gamma = s^*, p_x, p_y, d_{x^2-y^2} \\ &= \frac{2V}{L_x L_y} \sum_{\gamma} \varphi_{\mathbf{k}}^{(\gamma)} \varphi_{\mathbf{k}'}^{(\gamma)*} \end{aligned}$$

being $\varphi_{\mathbf{k}}^{(\gamma)}$ the reciprocal-space expressions for the form factors of Tab. 2.1, listed explicitly in Tab. 2.2, and $V_{\mathbf{k}\mathbf{k}'}^{(\gamma)}$ the symmetry-resolved components of the non-local attraction. Then the two-body potential has been decomposed in its planar symmetry components, each of which will naturally couple only to identically structured parameters in the full hamiltonian.

Define now the non-local gap function

$$\mathcal{V}_{\mathbf{k}} \equiv \sum_{\mathbf{k}'} V_{\mathbf{k}\mathbf{k}'} \langle \hat{\phi}_{\mathbf{k}'}^{\dagger} \rangle \tag{2.6}$$

one gets immediately

$$\hat{H}_V \simeq - \sum_{\mathbf{k}} \left[\mathcal{V}_{\mathbf{k}} \hat{\phi}_{\mathbf{k}} + \mathcal{V}_{\mathbf{k}}^* \hat{\phi}_{\mathbf{k}}^{\dagger} \right] \tag{2.7}$$

To assume symmetry is broken in a specific symmetry channel γ means precisely to assume $g_{ij} \propto \varphi_{ij}^{(\gamma)}$, which in turn implies $\langle \hat{\phi}_{\mathbf{k}} \rangle \propto \varphi_{\mathbf{k}}^{(\gamma)}$. Of course, in Eq. (2.6) only the γ component of the potential survives, implying the gap function acquires the same symmetry,

$$\begin{aligned} \mathcal{V}_{\mathbf{k}} &\propto \sum_{\mathbf{k}'} \frac{2V}{L_x L_y} \varphi_{\mathbf{k}}^{(\gamma)} \varphi_{\mathbf{k}'}^{(\gamma)*} \varphi_{\mathbf{k}'}^{(\gamma)} \\ &\propto \varphi_{\mathbf{k}}^{(\gamma)} \end{aligned}$$

where I used orthonormality of the $\varphi_{\mathbf{k}}^{(\gamma)}$ functions.

2.2.3 Local interaction and gap function

A very similar argument can be carried out for the local U term. Without delving in too many details, the local gap $\mathcal{U}_{\mathbf{k}}$ is given by

$$\mathcal{U}_{\mathbf{k}} \equiv \frac{U}{2L_xL_y}\sum_{\mathbf{k}}\langle\hat{\phi}_{\mathbf{k}}\rangle \tag{2.8}$$

evidently independent of $\mathbf{k}$, correctly. Identical considerations as in the above section hold for the local gap. The local part of the hamiltonian then gets

$$\hat{H}_U \simeq \sum_{\mathbf{k}}\left[\mathcal{U}_{\mathbf{k}}\hat{\phi}_{\mathbf{k}} + \mathcal{U}^*_{\mathbf{k}}\hat{\phi}^\dagger_{\mathbf{k}}\right] \tag{2.9}$$

and the full gap function is simply

$$\Delta_{\mathbf{k}} \equiv \mathcal{V}_{\mathbf{k}} - \mathcal{U}_{\mathbf{k}} \tag{2.10}$$

Notice here that the only possible topology here is s-wave; define trivially the s-wave component of the total two-body interaction,

$$V^{(s)} = -\frac{U}{2L_xL_y}$$

Then the full effective interaction is collected in

$$\begin{aligned}\hat{H}_U + \hat{H}_V &\simeq -\sum_{\gamma}\sum_{\mathbf{k},\mathbf{k}'} V^{(\gamma)}\varphi^{(\gamma)}_{\mathbf{k}}\varphi^{(\gamma)*}_{\mathbf{k}'}\left[\langle\hat{\phi}^\dagger_{\mathbf{k}}\rangle\hat{\phi}_{\mathbf{k}'} + \langle\hat{\phi}_{\mathbf{k}}\rangle\hat{\phi}^\dagger_{\mathbf{k}'}\right] \\ &= -\sum_{\mathbf{k}}\left[\Delta_{\mathbf{k}}\hat{\phi}_{\mathbf{k}} + \Delta^*_{\mathbf{k}}\hat{\phi}^\dagger_{\mathbf{k}}\right]\end{aligned}$$

The full self-consistency equation is given by

$$\Delta_{\mathbf{k}} \equiv \sum_{\mathbf{k}'}\left[V^{(s)} + V_{\mathbf{k}\mathbf{k}'}\right]\langle\hat{\phi}^\dagger_{\mathbf{k}'}\rangle \tag{2.11}$$

The gap function decomposes in symmetry channels as well,

$$\Delta_{\mathbf{k}} = \sum_{\gamma}\Delta^{(\gamma)}\varphi^{(\gamma)}_{\mathbf{k}}$$

If SC arises in a specific symmetry channel, $\Delta_{\mathbf{k}}$ will show the same symmetry. It follows, due to orthonormality and using Eq. (2.11),

$$\begin{aligned}\Delta^{(\gamma)} &= \frac{1}{L_xL_y}\sum_{\mathbf{k}}\varphi^{(\gamma)*}_{\mathbf{k}}\Delta_{\mathbf{k}} \\ &= \frac{1}{L_xL_y}\sum_{\mathbf{k}}\varphi^{(\gamma)*}_{\mathbf{k}}\sum_{\mathbf{k}'}\left[V^{(s)} + V_{\mathbf{k}\mathbf{k}'}\right]\langle\hat{\phi}^\dagger_{\mathbf{k}'}\rangle \\ &= \frac{1}{L_xL_y}\sum_{\mathbf{k}}\varphi^{(\gamma)*}_{\mathbf{k}}\sum_{\mathbf{k}'}V^{(\gamma')}\varphi^{(\gamma')}_{\mathbf{k}}\varphi^{(\gamma')*}_{\mathbf{k}'}\langle\hat{\phi}^\dagger_{\mathbf{k}'}\rangle \\ &= V^{(\gamma)}\sum_{\mathbf{k}}\varphi^{(\gamma)*}_{\mathbf{k}}\langle\hat{\phi}^\dagger_{\mathbf{k}}\rangle\end{aligned} \tag{2.12}$$

This result provides a set of self-consistency equations for each symmetry channel, listed in Tab. 2.3. Notice that to reconstruct self-consistently the full s-wave phase transition, the actual gap function is given by

$$\Delta^{(s)} + \Delta^{(s^*)}(c_x + c_y)$$

The s-wave transition is the only one equipped of both the local and the non-local parts. Within this structure, we are finally able to move to Nambu formalism.

Structure	Self-consistency equation	Graph
s-wave	$\Delta^{(s)} = -\dfrac{U}{2L_xL_y}\sum_{\mathbf{k}}\langle\hat{\phi}^\dagger_{\mathbf{k}}\rangle$	Fig. 2.2a
Extended s-wave	$\Delta^{(s^*)} = \dfrac{2V}{L_xL_y}\sum_{\mathbf{k}}(c_x+c_y)\langle\hat{\phi}^\dagger_{\mathbf{k}}\rangle$	Fig. 2.2b
p_x-wave	$\Delta^{(p_x)} = -\dfrac{2iV}{L_xL_y}\sum_{\mathbf{k}} s_x\langle\hat{\phi}^\dagger_{\mathbf{k}}\rangle$	Fig. 2.2c
p_y-wave	$\Delta^{(p_y)} = -\dfrac{2iV}{L_xL_y}\sum_{\mathbf{k}} s_y\langle\hat{\phi}^\dagger_{\mathbf{k}}\rangle$	Fig. 2.2d
$d_{x^2-y^2}$-wave	$\Delta^{(d)} = \dfrac{2V}{L_xL_y}\sum_{\mathbf{k}}(c_x-c_y)\langle\hat{\phi}^\dagger_{\mathbf{k}}\rangle$	Fig. 2.2e

Table 2.3 | Symmetry resolved self-consistency equations for the MFT parameters $\Delta^{(\gamma)}$, based on Eq. (2.11) and (2.12). By computing $\langle\hat{\phi}^\dagger_{\mathbf{k}}\rangle$, it is possible to reconstruct the various components of the gap function.

2.2.4 Nambu formalism and Bogoliubov transform

Define the Nambu spinor[4] as in BCS

$$\hat{\Psi}_{\mathbf{k}} \equiv \begin{bmatrix} \hat{c}_{\mathbf{k}\uparrow} \\ \hat{c}^\dagger_{-\mathbf{k}\downarrow} \end{bmatrix}$$

Evidently,

$$\phi_{\mathbf{k}} = \hat{\Psi}^\dagger_{\mathbf{k}}\begin{bmatrix} 0 & 1 \\ 0 & 0 \end{bmatrix}\hat{\Psi}_{\mathbf{k}} \qquad \phi^\dagger_{\mathbf{k}} = \hat{\Psi}^\dagger_{\mathbf{k}}\begin{bmatrix} 0 & 0 \\ 1 & 0 \end{bmatrix}\hat{\Psi}_{\mathbf{k}} \tag{2.13}$$

The full hamiltonian is then given by:

$$\hat{H} = \sum_{\mathbf{k}}\hat{\Psi}_{\mathbf{k}}h_{\mathbf{k}}\hat{\Psi}_{\mathbf{k}} \qquad h_{\mathbf{k}} \equiv \begin{bmatrix} \epsilon_{\mathbf{k}} & -\Delta^*_{\mathbf{k}} \\ -\Delta_{\mathbf{k}} & -\epsilon_{\mathbf{k}} \end{bmatrix} \tag{2.14}$$

Let τ^α for $\alpha = x, y, z$ be the Pauli matrices. Define:

$$\hat{s}^\alpha_{\mathbf{k}} \equiv \hat{\Psi}^\dagger_{\mathbf{k}}\tau^\alpha\hat{\Psi}_{\mathbf{k}} \quad \text{for} \quad \alpha = x, y, z$$

As can be shown easily, these operators realize spin-1/2 algebra. $\hat{H}$ represents an ensemble of L_xL_y independent spins subject to pseudo-magnetic fields. Note that, differently form App. **??** where the chemical potential is inserted later (because in Nambu formalism it accounts for a diagonal term) here the chemical potential is part of the z component of the pseudo-magnetic field, since

$$\begin{aligned} \hat{n}_{\mathbf{k}\uparrow} + \hat{n}_{-\mathbf{k}\downarrow} &= \hat{c}^\dagger_{\mathbf{k}\uparrow}\hat{c}_{\mathbf{k}\uparrow} + \hat{c}^\dagger_{-\mathbf{k}\downarrow}\hat{c}_{-\mathbf{k}\downarrow} \\ &= \hat{c}^\dagger_{\mathbf{k}\uparrow}\hat{c}_{\mathbf{k}\uparrow} - \hat{c}_{-\mathbf{k}\downarrow}\hat{c}^\dagger_{-\mathbf{k}\downarrow} + \mathbb{I} \\ &= \hat{\Psi}^\dagger_{\mathbf{k}}\tau^z\hat{\Psi}_{\mathbf{k}} + \mathbb{I} \end{aligned} \tag{2.15}$$

and then it follows

$$\begin{aligned} -\mu\hat{N} &= -\mu\sum_{\mathbf{k}\in\mathrm{BZ}}[\hat{n}_{\mathbf{k}\uparrow} + \hat{n}_{-\mathbf{k}\downarrow}] \\ &= -\mu\sum_{\mathbf{k}\in\mathrm{BZ}}\hat{\Psi}^\dagger_{\mathbf{k}}\tau^z\hat{\Psi}_{\mathbf{k}} - \mu L_xL_y \end{aligned}$$

[4] Notice that the spinor is here differently defined with respect to App. B, where because of the HF prevalence in mean-field decoupling the spinor components were homogeneously fermions creations or destructions.

Then, adding a term $-\mu\hat{N}$ to $\hat{H}$, apart from an irrelevant total energy increase, changes the pseudo-field whose explicit form becomes

$$\mathbf{b}_{\mathbf{k}} \equiv \begin{bmatrix} -\operatorname{Re}\{\Delta_{\mathbf{k}}\} \\ -\operatorname{Im}\{\Delta_{\mathbf{k}}\} \\ \epsilon_{\mathbf{k}} - \mu \end{bmatrix} \tag{2.16}$$

This hamiltonian behaves as an ensemble of spins in local magnetic fields precisely as in Eq. (B.4),

$$\hat{H} - \mu\hat{N} = \sum_{\mathbf{k}\in \mathrm{BZ}} \mathbf{b}_{\mathbf{k}} \cdot \hat{\mathbf{s}}_{\mathbf{k}} \quad \text{where} \quad \hat{\mathbf{s}}_{\mathbf{k}\sigma} = \begin{bmatrix} \hat{s}^x_{\mathbf{k}} \\ \hat{s}^y_{\mathbf{k}} \\ \hat{s}^z_{\mathbf{k}} \end{bmatrix} \tag{2.17}$$

Proceed as in App. **??** and diagonalize via a rotation,

$$d_{\mathbf{k}} \equiv \begin{bmatrix} -E_{\mathbf{k}} & \\ & E_{\mathbf{k}} \end{bmatrix} \quad \text{being} \quad E_{\mathbf{k}} \equiv \sqrt{\xi^2_{\mathbf{k}} + |\Delta_{\mathbf{k}}|^2}$$

and $\xi_{\mathbf{k}} \equiv \epsilon_{\mathbf{k}} - \mu$. Given the pseudoangles

$$\tan(2\theta_{\mathbf{k}}) \equiv \frac{|\Delta_{\mathbf{k}}|}{\epsilon_{\mathbf{k}}} \qquad \tan(2\zeta_{\mathbf{k}}) \equiv \frac{\operatorname{Im}\{\Delta_{\mathbf{k}}\}}{\operatorname{Re}\{\Delta_{\mathbf{k}}\}}$$

the general diagonalizer will be an orthogonal rotation matrix

$$\begin{aligned} W_{\mathbf{k}} &= e^{i\left(\theta_{\mathbf{k}} - \frac{\pi}{2}\right)\tau^y} e^{i\zeta_{\mathbf{k}}\tau^z} \\ &= \begin{bmatrix} -\sin\theta_{\mathbf{k}} & -\cos\theta_{\mathbf{k}} \\ \cos\theta_{\mathbf{k}} & -\sin\theta_{\mathbf{k}} \end{bmatrix} \begin{bmatrix} e^{i\zeta_{\mathbf{k}}} & \\ & e^{-i\zeta_{\mathbf{k}}} \end{bmatrix} \\ &= \begin{bmatrix} -\sin\theta_{\mathbf{k}} e^{i\zeta_{\mathbf{k}}} & -\cos\theta_{\mathbf{k}} e^{-i\zeta_{\mathbf{k}}} \\ \cos\theta_{\mathbf{k}} e^{i\zeta_{\mathbf{k}}} & -\sin\theta_{\mathbf{k}} e^{-i\zeta_{\mathbf{k}}} \end{bmatrix} \end{aligned} \tag{2.18}$$

given by a rotation of angle $\zeta_{\mathbf{k}}$ around the z axis, to align the x axis with the field projection onto the xy plane, followed by a rotation around the y axis to anti-align with the pseudo-field. The MFT-BCS solution is given by a degenerate Fermi gas at ground state, whose quasi-particles occupy two bands $\pm E_{\mathbf{k}}$ and their fermionic operators are given by

$$\hat{\gamma}^{(-)}_{\mathbf{k}} \equiv \left[W_{\mathbf{k}}\hat{\Psi}_{\mathbf{k}}\right]_1 \qquad \hat{\gamma}^{(+)}_{\mathbf{k}} \equiv \left[W_{\mathbf{k}}\hat{\Psi}_{\mathbf{k}}\right]_2$$

The diagonalization operators are given by

$$\hat{\Gamma}_{\mathbf{k}} \equiv W_{\mathbf{k}}\hat{\Psi}_{\mathbf{k}} \quad \text{where} \quad \hat{\Gamma}_{\mathbf{k}} = \begin{bmatrix} \hat{\gamma}^{(-)}_{\mathbf{k}} \\ \hat{\gamma}^{(+)}_{\mathbf{k}} \end{bmatrix}$$

then, using Eq. (B.9),

$$\left\langle [\hat{\Psi}^\dagger_{\mathbf{k}}]_i [\hat{\Psi}_{\mathbf{k}}]_j \right\rangle = [W_{\mathbf{k}}]_{1i}[W^\dagger_{\mathbf{k}}]_{j1} f\left(-E_{\mathbf{k}}; \beta, 0\right) + [W_{\mathbf{k}}]_{2i}[W^\dagger_{\mathbf{k}}]_{j2} f\left(E_{\mathbf{k}}; \beta, 0\right)$$

where in the Fermi-Dirac function chemical potential was set to zero, because it already was included in the diagonalized hamiltonian. Recalling Eq. (**??**), it follows

$$\langle \phi^\dagger_{\mathbf{k}} \rangle = [W_{\mathbf{k}}]_{11}[W^\dagger_{\mathbf{k}}]_{21} f\left(-E_{\mathbf{k}}; \beta, 0\right) + [W_{\mathbf{k}}]_{21}[W^\dagger_{\mathbf{k}}]_{22} f\left(E_{\mathbf{k}}; \beta, 0\right) \tag{2.19}$$

$$= \frac{1}{2}\sin\left(2\theta_{\mathbf{k}}\right) e^{i2\zeta_{\mathbf{k}}} \tanh\left(\frac{\beta E_{\mathbf{k}}}{2}\right) \tag{2.20}$$

The last passage obtained by computing the matrix element from the explicit form of $W_{\mathbf{k}}$ of Eq. (2.18) and by the simple relation

$$\begin{aligned} \frac{1}{e^{-x}+1} - \frac{1}{e^{x}+1} &= \frac{e^x - 1}{e^x + 1} \\ &= \tanh\left(\frac{x}{2}\right) \end{aligned}$$

Eqns. (2.19), (2.20) give us both the algorithmic formula (first row) and its theoretical counterpart (second row) to compute the order parameters in the HF approach at each point in k-space (k_x, k_y). We can finally derive the BCS self-consistency equation

$$\Delta_{\mathbf{k}} \equiv \frac{1}{2}\sum_{\mathbf{k}'}\left[V^{(s)} + V_{\mathbf{k}\mathbf{k}'}\right]\frac{|\Delta_{\mathbf{k}}|}{\sqrt{\xi_{\mathbf{k}}^2 + |\Delta_{\mathbf{k}}|^2}} e^{i\,\mathrm{Im}\{\Delta_{\mathbf{k}}\}/\,\mathrm{Re}\{\Delta_{\mathbf{k}}\}}\tanh\left(\frac{\beta}{2}\sqrt{\xi_{\mathbf{k}}^2 + |\Delta_{\mathbf{k}}|^2}\right) \tag{2.21}$$

The whole point of the HF algorithm is to find an iterative solution for each symmetry channel, using the self-consistency equation projection of Tab. 2.3.

Notice that the z component of the spin operators is related to density: using Eq. (B.9),

$$\langle\hat{\Psi}_{\mathbf{k}}^\dagger \tau^z \hat{\Psi}_{\mathbf{k}}\rangle = \left\langle[\hat{\Psi}_{\mathbf{k}}^\dagger]_1[\hat{\Psi}_{\mathbf{k}}]_1\right\rangle - \left\langle[\hat{\Psi}_{\mathbf{k}}^\dagger]_2[\hat{\Psi}_{\mathbf{k}}]_2\right\rangle$$

I proceed in as done previously, and from Eq. (2.15),

$$\begin{aligned}\langle\hat{n}_{\mathbf{k}\uparrow}\rangle + \langle\hat{n}_{-\mathbf{k}\downarrow}\rangle &= 1 + \langle\hat{\Psi}_{\mathbf{k}}^\dagger\tau^z\hat{\Psi}_{\mathbf{k}}\rangle \\ &= 1 + \left(|[W_{\mathbf{k}}]_{11}|^2 - |[W_{\mathbf{k}}]_{12}|^2\right) f\left(-E_{\mathbf{k}};\beta,0\right) \\ &\quad + \left(|[W_{\mathbf{k}}]_{21}|^2 - |[W_{\mathbf{k}}]_{22}|^2\right) f\left(E_{\mathbf{k}};\beta,0\right) \qquad (2.22) \\ &= 1 - \cos\left(2\theta_{\mathbf{k}}\right)\tanh\left(\frac{\beta E_{\mathbf{k}}}{2}\right) \qquad (2.23)\end{aligned}$$

The expectation value for the density is needed in order to extract the optimal chemical potential μ for the target density we aim to simulate at the given parametrization. This is numerically obtained by using Eq. (2.22) directly on the diagonalization matrix of $h_{\mathbf{k}}$.

2.2.5 A short comment on self-consistency

The Bogoliubov fermions in spinor representation satisfy obviously $\hat{\Psi}_{\mathbf{k}} = W_{\mathbf{k}}^\dagger\hat{\Gamma}_{\mathbf{k}}$. Consider e.g.

$$\langle\hat{c}_{\mathbf{k}\sigma}^\dagger\hat{c}_{-\mathbf{k}\sigma}^\dagger\rangle$$

which is a spin-symmetric anomalous Cooper pair. For simplicity, take $\sigma =\uparrow$. Expand:

$$\begin{aligned}\langle\hat{c}_{\mathbf{k}\uparrow}^\dagger\hat{c}_{-\mathbf{k}\uparrow}^\dagger\rangle &= \left\langle[\hat{\Psi}_{\mathbf{k}}^\dagger]_1[\hat{\Psi}_{-\mathbf{k}}^\dagger]_1\right\rangle \\ &= \left\langle[W_{\mathbf{k}}\hat{\Gamma}_{\mathbf{k}}^\dagger]_1[W_{-\mathbf{k}}\hat{\Gamma}_{-\mathbf{k}}^\dagger]_1\right\rangle\end{aligned}$$

This expectation value is taken over the ground-state, the latter being the vacuum of Γ fermions. Evidently the above expectation cannot assume non-zero values. Obviously the same holds for $\sigma =\downarrow$, and this argument explains why the Ferromagnetic terms of the hamiltonian decomposition do not contribute to Cooper instability. An identical argument, with the exchange

$$(\sigma,\sigma)\to(\uparrow,\downarrow) \quad\text{and}\quad (\mathbf{k},-\mathbf{k})\to(\mathbf{K}+\mathbf{k},\mathbf{K}-\mathbf{k}) \quad\text{with}\quad \mathbf{K}\neq\mathbf{0}$$

justifies why in Sec. 2.2.4 the only relevant contribution was given by $\mathbf{K} = \mathbf{0}$. In the next sections, the results of the self-consistent HF algorithm are exposed.

2.3 Results of the HF algorihtm

[To be continued...]

Appendix A

Superexchange and virtual hopping in Hubbard lattices

A key mechanism in AF phase formation in Hubbard lattice is superexchange. The AF phase is stabilized by spin fluctuations and second-order virtual hopping. The mechanism becomes clear enough by considering a 2-sites Hubbard toy model.

A.1 Virtual hopping in the 2-sites Hubbard lattice

Consider the toy model:

$$\hat{H} = -t\left\{\hat{c}^{\dagger}_{1\uparrow}\hat{c}_{2\uparrow} + \hat{c}^{\dagger}_{1\downarrow}\hat{c}_{2\downarrow} + \text{h.c.}\right\} + U\left\{\hat{n}_{1\uparrow}\hat{n}_{1\downarrow} + \hat{n}_{2\uparrow}\hat{n}_{2\downarrow}\right\}$$

with $i = 1, 2$ the site index. The two sites are represented in Fig. A.1. The two competing processes are:

1. electrons inter-sites hopping with amplitude $-t$;

2. local repulsion $+U$, acting when two anti-aligned electrons reside on the same site;

For an half-filled system, the Hilbert space is six-dimensional. I use the notation $|n_{1\uparrow}n_{1\downarrow}n_{2\uparrow}n_{2\downarrow}\rangle$ to indicate the six computational basis states:

$$\begin{array}{lll} |\psi_1\rangle \equiv |1010\rangle & |\psi_3\rangle \equiv |1001\rangle & |\psi_5\rangle \equiv |0011\rangle \\ |\psi_2\rangle \equiv |1100\rangle & |\psi_4\rangle \equiv |0110\rangle & |\psi_6\rangle \equiv |0101\rangle \end{array}$$

For example, the top panel of Fig. A.1 shows state $|\psi_2\rangle$.

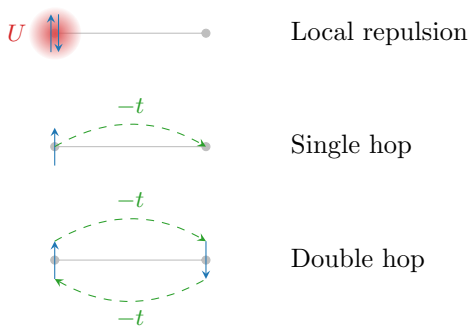

Figure A.1 | Two sites Hubbard model.

Structure	Eigenstate	Energy
Spin-1/2 singlet	$\frac{\lvert\phi_3\rangle - \lvert\phi_4\rangle}{\sqrt{2}}$	$E^- = \frac{U}{2} - \sqrt{\frac{U^2}{4} + 4t^2}$
Spin-1/2 triplet	$\lvert\phi_1\rangle, \frac{\lvert\phi_3\rangle + \lvert\phi_4\rangle}{\sqrt{2}}, \lvert\phi_6\rangle$	0
	$\frac{\lvert\phi_2\rangle - \lvert\phi_5\rangle}{\sqrt{2}}$	U
	$\frac{\lvert\phi_2\rangle + \lvert\phi_5\rangle}{\sqrt{2}}$	$E^+ = \frac{U}{2} + \sqrt{\frac{U^2}{4} + 4t^2}$

Table A.1 | List of exact eigenstates and relative energies for the 2-sites half-filled Hubbard model.

A.1.1 Exact solution of the half-filled model

The hamiltonian matrix is directly evaluated in this basis

$$H_{ij} = \langle\psi_i| \hat{H} |\psi_j\rangle \quad \Longrightarrow \quad H = \begin{bmatrix} 0 & & & & & \\ & U & -t & -t & & \\ & -t & & & -t & \\ & -t & & & -t & \\ & & -t & -t & U & \\ & & & & & 0 \end{bmatrix}$$

Empty slots in the matrix stand for zeros. Evidently the states $|\psi_1\rangle$ (both up) and $|\psi_6\rangle$ (both down) are zero-energy eigenstates. These states cannot realize electrons hopping because of Pauli principle. The internal 4×4 matrix is readily diagonalized by the means of a change of basis V,

$$V \begin{bmatrix} U & -t & -t & \\ -t & & & -t \\ -t & & & -t \\ & -t & -t & U \end{bmatrix} V^\dagger = \begin{bmatrix} E^- & & & \\ & 0 & & \\ & & U & \\ & & & E^+ \end{bmatrix}$$

Tab. A.1 shows the eigenvectors and relative eigenvalues obtained from diagonalization. The ground-state is the singlet state,

$$\frac{|\phi_3\rangle - |\phi_4\rangle}{\sqrt{2}} = \frac{|1010\rangle - |0101\rangle}{\sqrt{2}} = \frac{|\uparrow\downarrow\rangle - |\downarrow\uparrow\rangle}{\sqrt{2}}$$

of energy

$$E^- = \frac{U}{2} - \sqrt{\frac{U^2}{4} + 4t^2} \simeq -\frac{4t^2}{U}$$

the latter equality being true if $U \gg t$ (strong repulsion limit). The singlet state pairs with a spatially-symmetric (nodeless) wavefunction. The entire triplet (second row of Tab. A.1) remains at zero energy. Excited states are anti-symmetrized and symmetrized version of the polarized states $|\phi_1\rangle$ and $|\phi_6\rangle$.

A.1.2 Virtual hopping

The key feature of the singlet state is the one represented in the bottom panel of Fig. A.1: if the two electrons occupy separate sites and are anti-aligned, both "see" the other site as empty, thus free to hop to. [To be continued...]

Appendix B

Mean-Field Theory in Hubbard lattices

In this Appendix the Mean-Field solutions to the Hubbard hamiltonian,

$$\hat{H} = -t \sum_{\langle ij \rangle} \sum_{\sigma} \hat{c}^{\dagger}_{i\sigma} \hat{c}_{j\sigma} + U \sum_{i} \hat{n}_{i\uparrow} \hat{n}_{i\downarrow} \qquad t, U > 0$$

are described. The discussion is limited to the two-dimensional square lattice. The two-dimensional square lattice extension of the two-sites model can be studied by the means of Mean Field Theory. We have:

$$\begin{aligned} \hat{n}_{i\uparrow} \hat{n}_{i\downarrow} &= \left(\langle \hat{n}_{i\uparrow} \rangle + \delta \hat{n}_{i\uparrow} \right) \left(\langle \hat{n}_{i\downarrow} \rangle + \delta \hat{n}_{i\downarrow} \right) \\ &\simeq \langle \hat{n}_{i\uparrow} \rangle \langle \hat{n}_{i\downarrow} \rangle + \delta \hat{n}_{i\uparrow} \langle \hat{n}_{i\downarrow} \rangle + \langle \hat{n}_{i\uparrow} \rangle \delta \hat{n}_{i\downarrow} + \mathcal{O}\left(\delta n^2\right) \\ &= - \langle \hat{n}_{i\uparrow} \rangle \langle \hat{n}_{i\downarrow} \rangle + \hat{n}_{i\uparrow} \langle \hat{n}_{i\downarrow} \rangle + \langle \hat{n}_{i\uparrow} \rangle \hat{n}_{i\downarrow} + \mathcal{O}\left(\delta n^2\right) \end{aligned}$$

where $\delta \hat{n}_{i\sigma} \equiv \hat{n}_{i\sigma} - \langle \hat{n}_{i\sigma} \rangle$ and orders higher than first have been ignored, assuming negligible fluctuations around the equilibrium single-site population. The first term of the above three can be neglected at fixed particles number, being a pure energy shift.

B.1 Ferromagnetic solution

The Mean-Field Theory ferromagnetic solution prescribes an uniformly magnetized lattice,

$$\langle \hat{n}_{i\uparrow} \rangle = n + m \qquad \langle \hat{n}_{i\downarrow} \rangle = n - m$$

where n is the site electron density and m is the density unbalance, leading to a magnetization per site $2m$. The mean-field hamiltonian with these substitutions becomes:

$$\begin{aligned} \hat{H} &\simeq -t \sum_{\langle ij \rangle} \sum_{\sigma} \hat{c}^{\dagger}_{i\sigma} \hat{c}_{j\sigma} + U \sum_{i} \left[\hat{n}_{i\uparrow} \langle \hat{n}_{i\downarrow} \rangle + \langle \hat{n}_{i\uparrow} \rangle \hat{n}_{i\downarrow} \right] \\ &= -t \sum_{\langle ij \rangle} \sum_{\sigma} \hat{c}^{\dagger}_{i\sigma} \hat{c}_{j\sigma} + nU \sum_{i} \left[\hat{n}_{i\uparrow} + \hat{n}_{i\downarrow} \right] - mU \sum_{i} \left[\hat{n}_{i\uparrow} - \hat{n}_{i\downarrow} \right] \end{aligned}$$

Fourier transforming,

$$\begin{aligned} -t \sum_{\langle ij \rangle} \sum_{\sigma} \hat{c}^{\dagger}_{i\sigma} \hat{c}_{j\sigma} &= -2t \sum_{\mathbf{k}\sigma} \left[\cos(k_x) + \cos(k_y) \right] \hat{n}_{\mathbf{k}\sigma} \\ nU \sum_{i} \left[\hat{n}_{i\uparrow} + \hat{n}_{i\downarrow} \right] &= nU \sum_{\mathbf{k}\sigma} \hat{n}_{\mathbf{k}\sigma} \\ mU \sum_{i} \left[\hat{n}_{i\uparrow} - \hat{n}_{i\downarrow} \right] &= mU \sum_{\mathbf{k}\sigma} \left[\hat{n}_{\mathbf{k}\uparrow} - \hat{n}_{\mathbf{k}\downarrow} \right] \end{aligned}$$

having used adimensional lattice momenta. For a square lattice, the Brillouin Zone is delimited by

$$\mathbf{k} \in [-\pi, \pi] \times [-\pi, \pi]$$

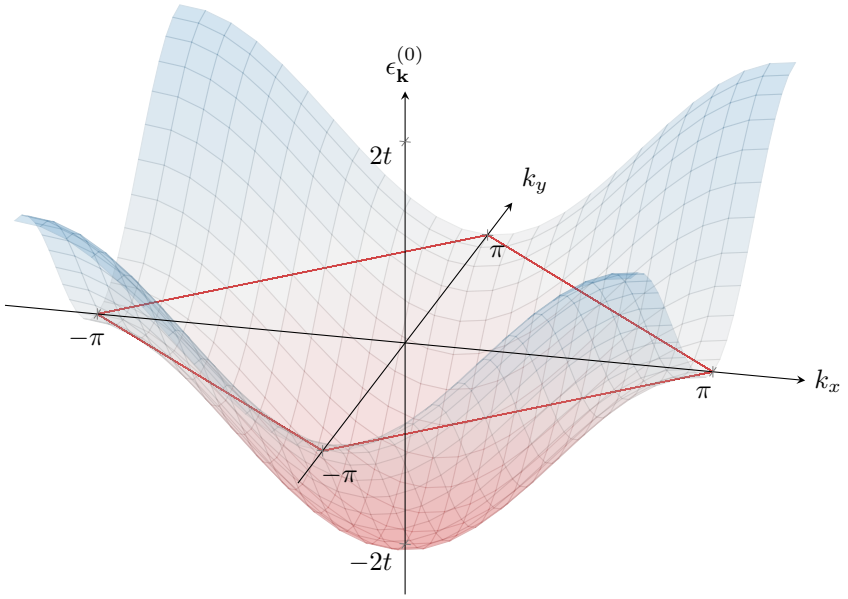

Figure B.1 | Depiction of the Hubbard square lattice hopping band $\epsilon^{(0)}_{\mathbf{k}} = -2t[\cos(k_x) + \cos(k_y)]$. The red lines mark the zero-energy intersection.

The hopping single-state energy is given by

$$\epsilon^{(0)}_{\mathbf{k}} = -2t\left[\cos(k_x) + \cos(k_y)\right]$$

represented as a band in Fig. B.1. At $U = 0$, the mean-field ferromagnetic state fills the band bottom-up. The single-state energy becomes:

$$\epsilon_{\mathbf{k}\uparrow} = U\,(n - m) - 2t\left[\cos(k_x) + \cos(k_y)\right]$$
$$\epsilon_{\mathbf{k}\downarrow} = U\,(n + m) - 2t\left[\cos(k_x) + \cos(k_y)\right]$$

Now it is a matter of finding the optimal value for m, minimizing the total energy at fixed filling $\rho = 2n$. Notice that said minimization is performed parametrically varying the magnetization m, inside the ferromagnetic-polarized space. As it turns out, for strong local repulsion $U/t \gg 1$, antiferromagnetic ordering is preferred. Comparison is needed in order to assess which magnetic ordering is preferred.

Consider the half-filling situation. An unpolarized system will have $n = 1/4$, $m = 0$: this implies $\langle \hat{n}_{i\uparrow} \rangle = \langle \hat{n}_{i\downarrow} \rangle = 1/4$. A perfectly up-ferromagnetic system, $n = 1/4$, $m = 1/4$: then $\langle \hat{n}_{i\uparrow} \rangle = 1/2$ and $\langle \hat{n}_{i\downarrow} \rangle = 0$. [To be continued...]

Unclear: numerically, it turns out the paramagnetic phase ($m = 0$) is preferred. Let $\Delta \equiv Um$ and ignore the constant contribution to energies Un: graphically, the $\uparrow$ band is shifted by Δ, the $\downarrow$ band by $-\Delta$. At half-filling the Fermi energy remains fixed. For each quadrant (top view of the bands), the DoS is inversion-symmetric with respect to the anti-diagonal (red lines in Fig. B.1), thus filling the bands bottom-up while performing the shifts should leave the total energy unchanged. Why is $m = 0$ preferred?

B.2 Antiferromagnetic solution

Consider now an AF mean-field solution. Let me change notation for a brief moment, indicating each site as

$$i \to \mathbf{r} = (x, y) \qquad x, y \in \mathbb{N}$$

The mean-field AF solution at half-filling is the uniform-modulated magnetization

$$m_{\mathbf{r}} = (-1)^{x+y} m \qquad m \in [-1, 1]$$

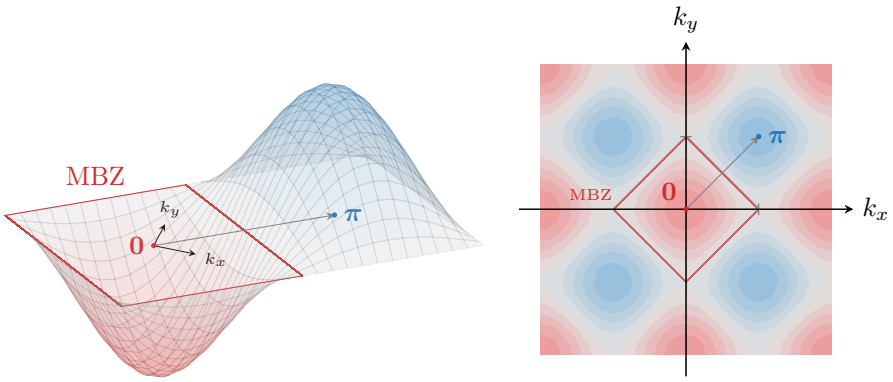

a | Alternative band. b | Contour plot.

Figure B.2 | Alternative depiction of the Hubbard square lattice hopping band previously reported in Fig. B.1. The Magnetic Brillouin Zone (MBZ) is delimited by the zero-energy contour and is indicated in figure. As it is evident, energy sign flips by taking a (π, π) translation in $\mathbf{k}$ space.

and a mean-field Ansatz

$$\langle \hat{n}_{\mathbf{r}\uparrow} \rangle = n + m_{\mathbf{r}} \qquad \langle \hat{n}_{\mathbf{r}\downarrow} \rangle = n - m_{\mathbf{r}}$$

With respect to the solution presented above, the only detail changing is the last term,

$$\hat{H} = -t \sum_{\langle \mathbf{r}\mathbf{r}' \rangle} \sum_{\sigma} \hat{c}^{\dagger}_{\mathbf{r}\sigma} \hat{c}_{\mathbf{r}'\sigma} + nU \sum_{\mathbf{r}} [\hat{n}_{\mathbf{r}\uparrow} + \hat{n}_{\mathbf{r}\downarrow}] - mU \sum_{\mathbf{r}} (-1)^{x+y} [\hat{n}_{\mathbf{r}\uparrow} - \hat{n}_{\mathbf{r}\downarrow}] \tag{B.1}$$

Fourier-transforming, the phase factor can be absorbed in the destruction operator inside of $\hat{n}_{\mathbf{r}\sigma}$:

$$\begin{aligned}
\sum_{\mathbf{r}} (-1)^{x+y} \hat{n}_{\mathbf{r}\sigma} &= \sum_{\mathbf{r}} (-1)^{x+y} \hat{c}^{\dagger}_{\mathbf{r}\sigma} \hat{c}_{\mathbf{r}\sigma} \\
&= \sum_{\mathbf{r}} e^{i\boldsymbol{\pi}\cdot\mathbf{r}} \frac{1}{L} \sum_{\mathbf{k}\in \mathrm{BZ}} e^{i\mathbf{k}\cdot\mathbf{r}} \hat{c}^{\dagger}_{\mathbf{k}\sigma} \frac{1}{L} \sum_{\mathbf{k}'\in \mathrm{BZ}} e^{-i\mathbf{k}'\cdot\mathbf{r}} \hat{c}_{\mathbf{k}'\sigma} \\
&= \sum_{\mathbf{k}\in \mathrm{BZ}} \sum_{\mathbf{k}'\in \mathrm{BZ}} \hat{c}^{\dagger}_{\mathbf{k}\sigma} \hat{c}_{\mathbf{k}'\sigma} \frac{1}{L^2} \sum_{\mathbf{r}} e^{-i[\mathbf{k}'-(\mathbf{k}+\boldsymbol{\pi})]\cdot\mathbf{r}} \\
&= \sum_{\mathbf{k}\in \mathrm{BZ}} \hat{c}^{\dagger}_{\mathbf{k}\sigma} \hat{c}_{\mathbf{k}+\boldsymbol{\pi}\sigma}
\end{aligned}$$

where $\boldsymbol{\pi} = (\pi, \pi)$. It follows:

$$mU \sum_{\mathbf{r}} (-1)^{x+y} [\hat{n}_{\mathbf{r}\uparrow} - \hat{n}_{\mathbf{r}\downarrow}] = \Delta \sum_{\mathbf{k}\in \mathrm{BZ}} \left[\hat{c}^{\dagger}_{\mathbf{k}\uparrow} \hat{c}_{\mathbf{k}+\boldsymbol{\pi}\uparrow} - \hat{c}^{\dagger}_{\mathbf{k}\downarrow} \hat{c}_{\mathbf{k}+\boldsymbol{\pi}\downarrow} \right] \quad \text{where} \quad \Delta \equiv mU$$

Consider the band of Fig. B.1 at half-filling. As does Fabrizio [3], the area delimited externally by the solid lines at zero energy is denominated "Magnetic Brillouin Zone" (MBZ). The periodicity of $\mathbf{k}$ space guarantees that the full BZ can be taken as well to be the one of Fig. B.2a. Then:

$$\begin{aligned}
\sum_{\mathbf{k}\in \mathrm{BZ}} \hat{c}^{\dagger}_{\mathbf{k}\uparrow} \hat{c}_{\mathbf{k}+\boldsymbol{\pi}\uparrow} &= \sum_{\mathbf{k}\in \mathrm{MBZ}} \left[\hat{c}^{\dagger}_{\mathbf{k}\uparrow} \hat{c}_{\mathbf{k}+\boldsymbol{\pi}\uparrow} + \hat{c}^{\dagger}_{\mathbf{k}+\boldsymbol{\pi}\uparrow} \hat{c}_{\mathbf{k}+2\boldsymbol{\pi}\uparrow} \right] \\
&= \sum_{\mathbf{k}\in \mathrm{MBZ}} \left[\hat{c}^{\dagger}_{\mathbf{k}\uparrow} \hat{c}_{\mathbf{k}+\boldsymbol{\pi}\uparrow} + \hat{c}^{\dagger}_{\mathbf{k}+\boldsymbol{\pi}\uparrow} \hat{c}_{\mathbf{k}\uparrow} \right]
\end{aligned} \tag{B.2}$$

and the same applies for spin $\downarrow$. Periodicity by shifts $2\boldsymbol{\pi}$ has been used. Now, define the Nambu spinors:

$$\hat{\Psi}_{\mathbf{k}\sigma} \equiv \begin{bmatrix} \hat{c}_{\mathbf{k}\sigma} \\ \hat{c}_{\mathbf{k}+\boldsymbol{\pi}\sigma} \end{bmatrix}$$

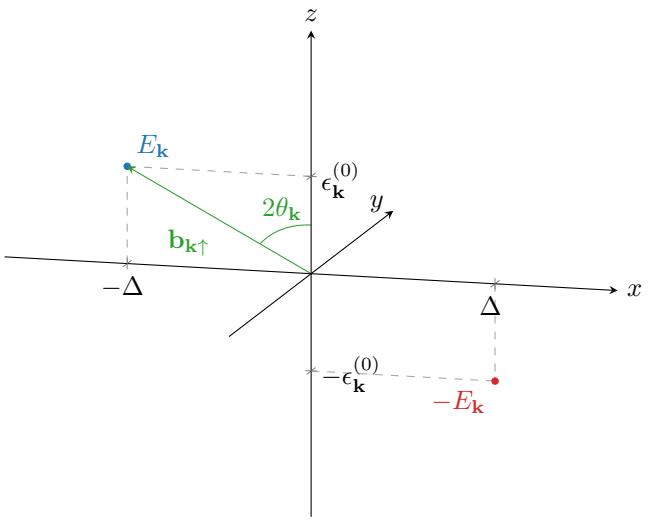

Figure B.3 | Pseudo-magnetic field originating from mean-field treatment of the square Hubbard hamiltonian. Here, only the $\sigma =\uparrow$

and a spin-wise gap,

$$\Delta_\uparrow = \Delta \qquad \Delta_\downarrow = -\Delta$$

At fixed filling, the U term is a pure energy shift, thus will be neglected. The kinetic term transforms as

$$\begin{aligned} -t \sum_{\langle ij \rangle} \sum_\sigma \hat{c}^\dagger_{i\sigma} \hat{c}_{j\sigma} &= \sum_{\mathbf{k}\in \mathrm{BZ}} \sum_\sigma \epsilon^{(0)}_{\mathbf{k}} \hat{c}^\dagger_{\mathbf{k}\sigma} \hat{c}_{\mathbf{k}\sigma} \\ &= \sum_{\mathbf{k}\in \mathrm{MBZ}} \sum_\sigma \left[\epsilon^{(0)}_{\mathbf{k}} \hat{c}^\dagger_{\mathbf{k}\sigma} \hat{c}_{\mathbf{k}\sigma} + \epsilon^{(0)}_{\mathbf{k}+\boldsymbol{\pi}} \hat{c}^\dagger_{\mathbf{k}+\boldsymbol{\pi}\sigma} \hat{c}_{\mathbf{k}+\boldsymbol{\pi}\sigma} \right] \\ &= \sum_{\mathbf{k}\in \mathrm{MBZ}} \sum_\sigma \epsilon^{(0)}_{\mathbf{k}} \left[\hat{c}^\dagger_{\mathbf{k}\sigma} \hat{c}_{\mathbf{k}\sigma} - \hat{c}^\dagger_{\mathbf{k}+\boldsymbol{\pi}\sigma} \hat{c}_{\mathbf{k}+\boldsymbol{\pi}\sigma} \right] \end{aligned}$$

In the second passage, the sum over the full BZ was written considering that the entirety of the zone is given by all the points in the MBZ plus their conjugates obtained by a $\boldsymbol{\pi}$ shift in the flipped band. As depicted in Fig. B.2a, kinetic energy is anti-periodic in $\mathbf{k}$ space by a vector $\boldsymbol{\pi}$. This anti-periodicity accounts for the minus sign arising in the third passage. The hamiltonian is then given by:

$$\hat{H} = \sum_{\mathbf{k}\in \mathrm{MBZ}} \sum_\sigma \hat{\Psi}^\dagger_{\mathbf{k}\sigma} h_{\mathbf{k}\sigma} \hat{\Psi}_{\mathbf{k}\sigma} \quad \text{being} \quad h_{\mathbf{k}\sigma} \equiv \begin{bmatrix} \epsilon^{(0)}_{\mathbf{k}} & -\Delta_\sigma \\ -\Delta_\sigma & -\epsilon^{(0)}_{\mathbf{k}} \end{bmatrix} \tag{B.3}$$

Notice: the Nambu hamiltonian is a 2×2 matrix over the MBZ – which is half the full BZ, coherently with a solution which essentially bipartites the lattice giving back a double sized unit cell.

The system ground-state is obtained by the means of a Bogoliubov rotation. The hamiltonian maps onto the simple one of a spin in a magnetic field,

$$h_{\mathbf{k}\sigma} = \epsilon^{(0)}_{\mathbf{k}} \tau^z - \Delta_\sigma \tau^x$$

being τ^α the Pauli matrices. Then, defining

$$\hat{s}^\alpha_{\mathbf{k}\sigma} \equiv \hat{\Psi}^\dagger_{\mathbf{k}\sigma} \tau^\alpha \hat{\Psi}_{\mathbf{k}\sigma} \quad \text{and} \quad \mathbf{b}_{\mathbf{k}\sigma} \equiv \begin{bmatrix} -\Delta_\sigma \\ 0 \\ \epsilon^{(0)}_{\mathbf{k}} \end{bmatrix}$$

one gets:

$$\hat{H} = \sum_{\mathbf{k}\in \mathrm{MBZ}} \sum_\sigma \mathbf{b}_{\mathbf{k}\sigma} \cdot \hat{\mathbf{s}}_{\mathbf{k}\sigma} \quad \text{where} \quad \hat{\mathbf{s}}_{\mathbf{k}\sigma} = \begin{bmatrix} \hat{s}^x_{\mathbf{k}\sigma} \\ \hat{s}^y_{\mathbf{k}\sigma} \\ \hat{s}^z_{\mathbf{k}\sigma} \end{bmatrix} \tag{B.4}$$

The hamiltonian represents a system of spins subject to local magnetic fields, each tilted by an angle $\tan(2\theta_{\mathbf{k}\sigma}) = \Delta_\sigma/\epsilon^{(0)}_{\mathbf{k}}$, as sketched in Fig. B.3. At any finite temperature, the ground-state of such a system is well-known. Diagonalization of each $h_{\mathbf{k}\sigma}$ is obtained trivially by a simple rotation around the y axis:

$$d_{\mathbf{k}\sigma} = W_{\mathbf{k}\sigma} h_{\mathbf{k}\sigma} W^\dagger_{\mathbf{k}\sigma}$$

where

$$d_{\mathbf{k}\sigma} = \begin{bmatrix} -E_{\mathbf{k}} & \\ & E_{\mathbf{k}} \end{bmatrix} \quad \text{and} \quad W_{\mathbf{k}\sigma} = \exp\left\{ i \frac{2\theta_{\mathbf{k}\sigma} - \pi}{2} \tau^y \right\}$$

Note that rotation is taken to be of an angle $2\theta_{\mathbf{k}\sigma} - \pi$ in order to anti-align the pseudo-spin with the magnetic field of Fig. B.3 and thus order the eigenvalues as in $d_{\mathbf{k}\sigma}$, with the smaller one in the top-left corner of the matrix and the larger one in the bottom-right corner. The explicit form of the transformation matrix is thus

$$W_{\mathbf{k}\sigma} = \begin{bmatrix} \cos\theta_{\mathbf{k}\sigma} & -\sin\theta_{\mathbf{k}\sigma} \\ \sin\theta_{\mathbf{k}\sigma} & \cos\theta_{\mathbf{k}\sigma} \end{bmatrix} \begin{bmatrix} & -1 \\ 1 & \end{bmatrix} = \begin{bmatrix} -\sin\theta_{\mathbf{k}\sigma} & -\cos\theta_{\mathbf{k}\sigma} \\ \cos\theta_{\mathbf{k}\sigma} & -\sin\theta_{\mathbf{k}\sigma} \end{bmatrix} \tag{B.5}$$

Eigenvalues are:

$$E_{\mathbf{k}} \equiv \sqrt{\epsilon^2_{\mathbf{k}} + |\Delta_\sigma|^2}$$

(superscript "(0)" has been dropped momentarily). Notice that the presence of an absolute value makes the eigenvalues independent of the σ index. Eigenvector fermion operators are obtained simply as:

$$\hat{\Gamma}_{\mathbf{k}\sigma} = W_{\mathbf{k}\sigma} \hat{\Psi}_{\mathbf{k}\sigma}$$

The $\hat{\Gamma}$ spinor operators are effectively free fermionic spinor fields and as such must be treated. Note that:

$$\begin{aligned} N &= \sum_{\mathbf{k}\sigma} \langle \hat{n}_{\mathbf{k}\sigma} \rangle \\ &= \sum_{\sigma} \sum_{\mathbf{k}\in \mathrm{MBZ}} \langle \hat{n}_{\mathbf{k}\sigma} + \hat{n}_{\mathbf{k}+\boldsymbol{\pi}\sigma} \rangle \\ &= \sum_{\sigma} \sum_{\mathbf{k}\in \mathrm{MBZ}} \left\langle \hat{\Gamma}^\dagger_{\mathbf{k}\sigma} \hat{\Gamma}_{\mathbf{k}\sigma} \right\rangle \\ &= 2\left[f\left(-E_{\mathbf{k}\sigma}; \beta, \mu\right) + f\left(E_{\mathbf{k}\sigma}; \beta, \mu\right) \right] \end{aligned} \tag{B.6}$$

being f be the Fermi-Dirac distribution at inverse temperature β and chemical potential μ,

$$f(\epsilon; \beta, \mu) = \frac{1}{e^{\beta(\epsilon-\mu)} + 1}$$

Eq. (B.6)holds because the Φ fields represent free fermions and the spin DoF is just a degeneracy factor. Next sections are devoted to simplify the above theoretical results in order to obtain an algorithmic estimation for the magnetization m, which is just the AF instability order parameter.

B.2.1 Theoretical mean-field solution

A convergence algorithm can be designed to find the Hartree-Fock solution to the model. Ultimately, we aim to extract m self-consistently. Since

$$\begin{aligned} m &= \frac{1}{2L^2} \sum_{\mathbf{r}} (-1)^{x+y} \langle \hat{n}_{\mathbf{r}\uparrow} - \hat{n}_{\mathbf{r}\downarrow} \rangle \\ &= \frac{1}{2L^2} \sum_{\mathbf{k}\in \mathrm{BZ}} \left\langle \hat{c}^\dagger_{\mathbf{k}\uparrow} \hat{c}_{\mathbf{k}+\boldsymbol{\pi}\uparrow} - \hat{c}^\dagger_{\mathbf{k}\downarrow} \hat{c}_{\mathbf{k}+\boldsymbol{\pi}\downarrow} \right\rangle \\ &= \frac{1}{2L^2} \sum_{\mathbf{k}\in \mathrm{MBZ}} \left\langle \left(\hat{c}^\dagger_{\mathbf{k}\uparrow} \hat{c}_{\mathbf{k}+\boldsymbol{\pi}\uparrow} + \hat{c}^\dagger_{\mathbf{k}+\boldsymbol{\pi}\uparrow} \hat{c}_{\mathbf{k}\uparrow} \right) - \left(\hat{c}^\dagger_{\mathbf{k}\downarrow} \hat{c}_{\mathbf{k}+\boldsymbol{\pi}\downarrow} + \hat{c}^\dagger_{\mathbf{k}+\boldsymbol{\pi}\downarrow} \hat{c}_{\mathbf{k}\downarrow} \right) \right\rangle \end{aligned}$$

In the last passage, Eq. (B.2) has been used. Then magnetization can be computed simply as

$$m = \frac{1}{2L^2} \sum_{\mathbf{k}\in \mathrm{MBZ}} \left[\left\langle \hat{\Psi}^\dagger_{\mathbf{k}\uparrow} \tau^x \hat{\Psi}_{\mathbf{k}\uparrow} \right\rangle - \left\langle \hat{\Psi}^\dagger_{\mathbf{k}\downarrow} \tau^x \hat{\Psi}_{\mathbf{k}\downarrow} \right\rangle \right] \tag{B.7}$$

In this equation, spin expectation values appear:

$$\left\langle \hat{\Psi}^\dagger_{\mathbf{k}\sigma} \tau^x \hat{\Psi}_{\mathbf{k}\sigma} \right\rangle = \langle \hat{s}^x_{\mathbf{k}\sigma} \rangle$$

Now discussion is divided in two parts: zero temperature and finite temperature.

Zero temperature solution

For a spin system at zero temperature, the spin operator expectation value anti-aligns with the external field,

$$\langle \hat{s}^x_{\mathbf{k}\sigma} \rangle = \sin(2\theta_{\mathbf{k}\sigma})$$

(see Fig. B.3). Now, since $\Delta_\downarrow = -\Delta_\uparrow$, it follows

$$\theta_{\mathbf{k}\downarrow} = -\theta_{\mathbf{k}\uparrow} \equiv \theta_{\mathbf{k}}$$

Then, from Eq. (B.7)

$$\begin{aligned} m &= \frac{1}{L^2} \sum_{\mathbf{k}\in \mathrm{MBZ}} \sin(2\theta_{\mathbf{k}}) \\ &= \frac{1}{2L^2} \sum_{\mathbf{k}\in \mathrm{BZ}} \sin(2\theta_{\mathbf{k}}) \end{aligned}$$

The last passage is due to the fact that the sum over the MBZ can be performed identically over $\mathrm{BZ} \setminus \mathrm{MBZ}$ and yield the same result. This is because of the lattice periodicity in reciprocal space. Then, finally:

$$m = \frac{1}{L^2} \sum_{\mathbf{k}\in \mathrm{BZ}} [W_{\mathbf{k}\uparrow}]_{11} [W^\dagger_{\mathbf{k}\uparrow}]_{21} \tag{B.8}$$

where $\sin(2\theta_{\mathbf{k}}) = 2\sin\theta_{\mathbf{k}} \cos\theta_{\mathbf{k}}$ has been used. As will become clear in next section, the sudden appearance of matrix elements of W is not casual.

Finite temperature solution

At finite temperature β, discussion is analogous to the section above. Here will be treated somewhat more theoretically. Define the generic order parameter:

$$\Delta_{ij}(\mathbf{k}\sigma) \equiv \left\langle [\hat{\Psi}^\dagger_{\mathbf{k}\sigma}]_i [\hat{\Psi}_{\mathbf{k}\sigma}]_j \right\rangle$$

In last section, the relevant indices (i, j) were $(1, 2)$ and $(2, 1)$. Transform this order parameter,

$$\begin{aligned} \Delta_{ij}(\mathbf{k}\sigma) &= \sum_{i'j'} \left\langle [\hat{\Gamma}^\dagger_{\mathbf{k}\sigma}]_{i'} [W_{\mathbf{k}\sigma}]_{i'i} [W^\dagger_{\mathbf{k}\sigma}]_{jj'} [\hat{\Gamma}_{\mathbf{k}\sigma}]_{j'} \right\rangle \\ &= \sum_{i'j'} [W_{\mathbf{k}\sigma}]_{i'i} [W^\dagger_{\mathbf{k}\sigma}]_{jj'} \left\langle [\hat{\Gamma}^\dagger_{\mathbf{k}\sigma}]_{i'} [\hat{\Gamma}_{\mathbf{k}\sigma}]_{j'} \right\rangle \\ &= \sum_{i'j'} [W_{\mathbf{k}\sigma}]_{i'i} [W^\dagger_{\mathbf{k}\sigma}]_{jj'} \delta_{i'j'} f\left([d_{\mathbf{k}\sigma}]_{i'i'}; \beta, \mu\right) \\ &= \sum_{\ell=1}^{2} [W_{\mathbf{k}\sigma}]_{\ell i} [W^\dagger_{\mathbf{k}\sigma}]_{j\ell} f\left((-1)^\ell E_{\mathbf{k}\sigma}; \beta, \mu\right) \\ &= [W_{\mathbf{k}\sigma}]_{1i} [W^\dagger_{\mathbf{k}\sigma}]_{j1} f\left(-E_{\mathbf{k}\sigma}; \beta, \mu\right) + [W_{\mathbf{k}\sigma}]_{2i} [W^\dagger_{\mathbf{k}\sigma}]_{j2} f\left(E_{\mathbf{k}\sigma}; \beta, \mu\right) \end{aligned} \tag{B.9}$$

In the second passage this distribution appeared because an expectation value over a gas of free Φ fermions was taken. Such an expectation value admits no off-diagonal values, hence the $\delta_{i'j'}$. The

diagonal entries are precisely the definition of the Fermi-Dirac distribution for the given energy. At zero temperature and half-filling, the lower band $-E_{\mathbf{k}}$ is completely filled while the upper band $E_{\mathbf{k}}$ is empty. Substituting $f = 1$ in the first term of line (B.9), $f = 0$ in the second and summing Δ_{12} and Δ_{21} as done in Eq. (B.7), it's easy to derive the result of Eq. (B.8). At finite temperature, following the lead of the above paragraph, the antiferromagnetic instability order parameter m will be given simply by

$$m = \frac{1}{2L^2} \sum_{\mathbf{k}\in \mathrm{BZ}} \sum_{\ell=1}^{2} [W_{\mathbf{k}\uparrow}]_{\ell 1} [W^{\dagger}_{\mathbf{k}\uparrow}]_{2\ell} f\left((-1)^{\ell} E_{\mathbf{k}\sigma}; \beta, \mu\right) \tag{B.10}$$

Then: mean-field approximations yield an estimate for the magnetization at a given temperature and chemical potential just by carefully combining the elements of the diagonalizing matrix W of each Bogoliubov matrix $h_{\mathbf{k}\sigma}$.

B.2.2 Hartree-Fock algorithm in reciprocal space

The above sections offers a self-consistency equation for the magnetization m; W is determined by m indeed. Then a self-consistent algorithm to search for a self consistent estimate for m may be sketched:

0. Algorithm setup: initialize a counter $i = 1$ and choose:
   - the local repulsion U/t or equivalently the hopping amplitude t/U;
   - the coarse-graining of the BZ, which is, fix L_x and L_y. Then
     $$k_x = 2\pi n_x / L_x \qquad k_y = 2\pi n_y / L_y$$
     where $-L_j/2 \leq n_j \leq L_j/2$, $n_j \in \mathbb{Z}$;
   - the density n or equivalently the doping $\delta \equiv n - 0.5$;
   - the inverse temperature β;
   - the number of iterations $p \in \mathbb{N}$;
   - the mixing parameter $g \in [0, 1]$;
   - the tolerance parameters $\Delta_m, \Delta_n \in \mathbb{R}$ (respectively for magnetization and density);
1. Select a random starting value $m_0 \in [-(1-n), 1-n]$;
2. For each slot of the BZ, initialize the appropriate 2×2 matrix $h_{\mathbf{k}\uparrow}$ as in Eq. (B.3);
3. For the given hamiltonian, find the optimal chemical potential μ as follows:
   a) Diagonalize $h_{\mathbf{k}\uparrow}[m_0, U]$ and obtain its eigenvalues $\pm E_k[m_0, U]$;
   b) Define the function of the chemical potential μ,
   $$\delta n(\mu; \beta, m_0, U) \equiv 2\left[f\left(-E_{\mathbf{k}\sigma}[U, m_0]; \beta, \mu\right) + f\left(E_{\mathbf{k}\sigma}[U, m_0]; \beta, \mu\right)\right] - n$$
   c) Find the root of δn,
   $$\delta n(\mu_0) = 0$$
   Then μ_0 is the chemical potential which, at magnetization m_0, realizes the best approximation of density n;
4. Diagonalize the matrix $h_{\mathbf{k}\uparrow}$ and obtain $d_{\mathbf{k}\uparrow}$;
5. Compute m using Eq. (B.10) with chemical potential μ_0 and update the counter, $i \to i + 1$;
6. Check if $|m - m_0| \leq \delta_m$:
   - If yes, halt;
   - If not: check if $i > p$

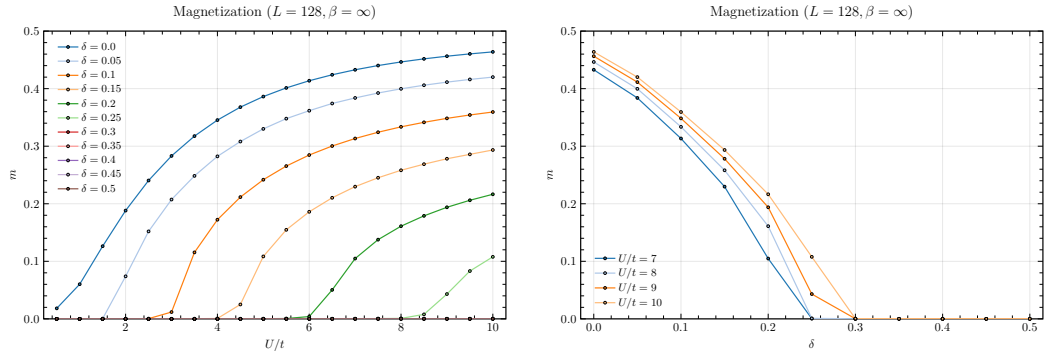

a | Local repulsion U/t depencence.

b | Doping $\delta = n - 0.5$ dependence.

Figure B.4 | Plots of the zero-temperature AF instability order parameter m as a function of both the local repulsion U/t (Fig. B.4a) and the doping $\delta = n - 1/2$ (Fig. B.4b).

- If yes, halt and consider choosing better tolerance and model parameters;
- If not, define

$$m_0 = gm + (1 - g)m_0$$

(logical assignment notation used) and repeat from step 2.

In next section some results are briefly shown.

Results

The algorithm sketched in the above paragraph was ran with the following setup:

```
UU = [U for U in 0.5:0.5:10.0]          # Local repulsions
LL = [2^x for x in 5:7]                 # Lattice sizes
dd = [d for d in 0.0:0.05:0.5]          # Dopings
bb = [0.1, 1.0, 10.0, 50.0, Inf]        # Inverse temperatures
p = 100                                 # Max number of iterations
dm = 1e-4                               # Tolerance on magnetization
dn = 1e-2                               # Tolerance on density
g = 0.5                                 # Mixing parameter
```

In Fig. B.4 plots at $\beta = \infty$ of the magnetization m are reported. As is evident in Fig. B.4a, disrupts AF ordering; the horizontal asymptote lowers as δ gets bigger, a mere consequence of the fact that the free space at each single-particle state in k-space shrinks as density increases; also, for $\delta > 0$, a finite magnetization m exists only for $U \geq U_c[\delta]$ (a critical value parametrically dependent on doping). Fig. B.4b shows the dependence of magnetization on doping at various fixed local repulsions U: once again, to dope the material disrupt AF ordering. Identical analysis have been performed for finite temperatures, leading to analogous results as long as $\beta \gtrsim 10$ and to $m \simeq 0$ for higher temperatures (predictably).

B.2.3 An alternative (less efficient) real-space approach

The theoretical derivation of the above paragraphs offers a simple description of the system anti-ferromagnetic instability as the instauration of a ground-state of quasiparticles. Here a self-consistent algorithmic extraction of the expected magnetization is presented, following [7]. Note that this algorithm is by far the least efficient, being performed in real space with dimensional exponential scaling in terms of computational time. It is here presented just for completeness as an alternative derivation. This algorithm can become useful for simulations not preserving space-translational invariance, e.g. introducing some degree of disorder. Consider a square lattice of

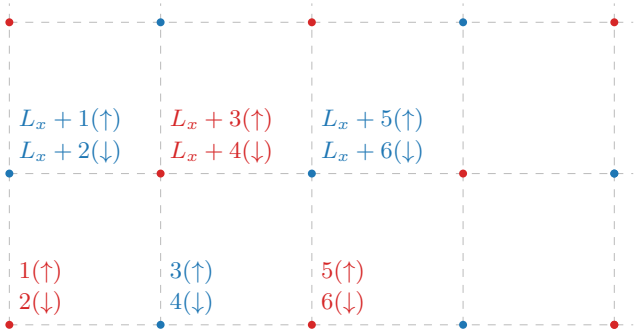

Figure B.5 | Schematics of the site ordering on a square lattice performed by sweeping along rows. Left-bottom side is one corner of the lattice. Red sites are characterized by $x + y$ being odd, blue sites by being even. The number reported near to each site is the α entry in the matrix representation for a finite square lattice.

$L_x \times L_y$ sites: the hamiltonian will be a matrix of dimension $2L_xL_y \times 2L_xL_y$,

$$[\hat{H}]_{(\mathbf{r}\sigma)(\mathbf{r}'\sigma')} = \langle\Omega|\hat{c}_{\mathbf{r}\sigma}\hat{H}\hat{c}^{\dagger}_{\mathbf{r}'\sigma'}|\Omega\rangle$$

For simplicity, in the following $D \equiv 2L_xL_y$. In this context, the following convention is used: the rows/column index entry $\alpha = (\mathbf{r}\sigma)$ is associated to a specific site $\mathbf{r} = (x, y)$ and spin σ through the relation

$$\alpha = 2j_{\mathbf{r}} - \delta_{\sigma=\uparrow} \quad \text{where} \quad j_{\mathbf{r}} = x + (y-1)L_x$$

Let me break this through. For each site $\mathbf{r}$, two sequential indices are provided ($2j_{\mathbf{r}} - 1$, hosting spin $\uparrow$, and $2j_{\mathbf{r}}$, hosting spin $\downarrow$). $j_{\mathbf{r}}$ just orders the site rows-wise. This way, $(x, 1)$ is assigned to $j_{(x,1)} = x$, while its NN one site above $(x, 2)$ is assigned to an entry shifted by L_x, $j_{(x,2)} = x + L_x$. This is just a way of counting the site of a finite square lattice by sweeping along a row and then moving to the row above. Fig. B.5 reports a scheme of the used site ordering.

Within this convention, matrix elements $H_{\alpha\beta}$ are defined by:

- If $\sigma = \sigma'$ and $\mathbf{r}$, $\mathbf{r}'$ are NN, the matrix entry is $-t$. In terms of the used greek indices, α and β satisfy said requirement if $|\alpha - \beta| = 2$ (horizontal hopping) or $|\alpha - \beta| = 2L_x$ (vertical hopping). Along column α of the hamiltonian matrix, the elements $-t$ appear at positions

$$(\alpha \pm 2L_x) \mod D \quad \text{and} \quad (\alpha \pm 2) \mod D$$

- If $\mathbf{r} = \mathbf{r}'$ and $\sigma = \sigma'$ (along the diagonal), the local interaction with the mean field is given by the matrix element

$$-mU \times (-1)^{x+y} \times (-1)^{\delta_{\sigma=\downarrow}}$$

Starting from a given entry α, $j_{\mathbf{r}}$ is retrieved simply by $j_{\mathbf{r}} = \lfloor \alpha/2 \rfloor$, and then

$$x + y = (j_{\mathbf{r}} + 1) - \left\lfloor \frac{j_{\mathbf{r}}}{L_x} \right\rfloor (L_x - 1)$$

Then the $j_{\mathbf{r}}$-th 2×2 block along the diagonal will be given by

$$(-1)^{x+y} \underbrace{\begin{bmatrix} -mU & \\ & mU \end{bmatrix}}_{\mathcal{B}}$$

Note that the resulting block diagonal contribution to the hamiltonian is shaped like follows (assume L_x to be even):

$$\begin{array}{c} \\ 1 \\ 2 \\ \vdots \\ L_x-1 \\ L_x \\ L_x+1 \\ L_x+2 \\ \vdots \end{array}\!\!\begin{array}{c} \begin{array}{cccccccc} 1 & 2 & \cdots & L_x-1 & L_x & L_x+1 & L_x+2 & \cdots \end{array} \\ \begin{bmatrix} \mathcal{B} & & & & & & & \\ & -\mathcal{B} & & & & & & \\ & & \ddots & & & & & \\ & & & \mathcal{B} & & & & \\ & & & & -\mathcal{B} & & & \\ & & & & & -\mathcal{B} & & \\ & & & & & & \mathcal{B} & \\ & & & & & & & \ddots \end{bmatrix} \end{array}$$

Along the same row, on the diagonal the 2×2 blocks $\mathcal{B}$ alternate signs; changing row (in the example above, at positions L_x, L_x+1), due to the anti-ferromagnetic configuration of local mean-fields, an additional -1 is included. If L_x is taken to be odd, the diagonal blocks just alternate signs all the way.

These prescriptions allow to build from scratch the hamiltonian matrix. After that, diagonalization provides D orthonormal eigenvectors $\mathbf{v}^\ell \in \mathbb{C}^{D\times D}$ with $\ell = 1, \cdots, D$, each associated to a precise eigenvalue $\epsilon^\ell \in \mathbb{R}$. At equilibrium, electrons will fill up the energy eigenstates according to,

$$\langle \hat{n}_{\mathbf{r}\sigma} \rangle = \sum_{\ell=1}^{D} \left| v_\alpha^\ell \right|^2 f(\epsilon^\ell; \beta, \mu) \quad \text{where} \quad \alpha = (\mathbf{r}\sigma)$$

For a fixed filling $n = N/D$, the chemical potential must satisfy

$$\begin{aligned} n &= \frac{1}{D} \sum_{\mathbf{r}\sigma} \langle \hat{n}_{\mathbf{r}\sigma} \rangle \\ &= \frac{1}{D} \sum_{\mathbf{r}\sigma} \sum_{\ell=1}^{D} \left| v_\alpha^\ell \right|^2 f(\epsilon^\ell; \beta, \mu) \\ &= \frac{1}{D} \sum_{\ell=1}^{D} f(\epsilon^\ell; \beta, \mu) \end{aligned}$$

since the $\mathbf{v}^\ell$ eigenvectors are orthonormal. The chemical potential for the half-filled model is already known to be

$$\mu\big|_{n=1/2} = -\frac{U}{2}$$

as evident from Eq. (B.1). Average magnetization is then given by

$$\begin{aligned} m &= \frac{1}{D} \sum_{\mathbf{r}} (-1)^{x+y} \left[\langle \hat{n}_{\mathbf{r}\uparrow} \rangle - \langle \hat{n}_{\mathbf{r}\downarrow} \rangle \right] \\ &= \frac{1}{D} \sum_{\lambda=1}^{D/2} (-1)^{(\lambda+1)-\lfloor \lambda/L_x \rfloor (L_x-1)} \sum_{\ell=1}^{D} \left[\left| v_{2\lambda-1}^\ell \right|^2 - \left| v_{2\lambda}^\ell \right|^2 \right] f(\epsilon^\ell; \beta, \mu) \end{aligned} \tag{B.11}$$

since $\mathbf{r}\uparrow$ is associated to an odd index entry, while $\mathbf{r}\downarrow$ to the following even entry. The associated HF algorithm is identical to the one presented in Sec. B.2.2, with the following substitutions:

2. Initialize the hamiltonian matrix $H_{\alpha\beta}$ matrix according to the initialized m_0 and the site indexing rules of Fig. B.5;

4. Diagonalize the matrix associated to the operator $\hat{H}_{\alpha\beta} - \mu\hat{N}$ collecting the $\mathbf{v}^\ell$ eigenvectors;

5. Compute m using Eq. (B.11) and update the counter, $i \to i+1$;

Bibliography

[1] Zhangkai Cao et al. *p-wave superconductivity induced by nearest-neighbor attraction in the square-lattice extended Hubbard model*. en. arXiv:2408.01113 [cond-mat]. Jan. 2025. DOI: 10.48550/arXiv.2408.01113. URL: http://arxiv.org/abs/2408.01113 (visited on 03/15/2025).

[2] Piers Coleman. *Introduction to Many-Body Physics*. Cambridge University Press, 2015.

[3] Michele Fabrizio. *A Course in Quantum Many-Body Theory*. Springer, 2022.

[4] Gabriele Giuliani and Giovanni Vignale. *Quantum Theory of the Electron Liquid*. Cambridge University Press, 2005.

[5] Giuseppe Grosso and Giuseppe Pastori Parravicini. *Solid State Physics*. Second Edition. Academic Press, 2014.

[6] J. E. Hirsch. "Two-dimensional Hubbard model: Numerical simulation study". In: *Phys. Rev. B* 31 (7 Apr. 1985), pp. 4403–4419. DOI: 10.1103/PhysRevB.31.4403. URL: https://link.aps.org/doi/10.1103/PhysRevB.31.4403.

[7] Robin Scholle et al. "Comprehensive mean-field analysis of magnetic and charge orders in the two-dimensional Hubbard model". In: *Phys. Rev. B* 108 (3 July 2023), p. 035139. DOI: 10.1103/PhysRevB.108.035139. URL: https://link.aps.org/doi/10.1103/PhysRevB.108.035139.